Journal of Cosmology and Astroparticle Physics
An IOP and SISSA journal

Received: *July 30, 2025*
Revised: *December 11, 2025*
Accepted: *December 22, 2025*
Published: *February 18, 2026*

Neutrino non-radiative decay in matter: constraints and prospects

Pilar Iváñez-Ballesteros[a] **and Maria Cristina Volpe**[b,*]

[a] *Université Paris Cité, Astroparticule et Cosmologie, 10 rue A. Domon et L. Duquet, F-75013 Paris, France*
[b] *CNRS, Université Paris Cité, Astroparticule et Cosmologie, 10 rue A. Domon et L. Duquet, F-75013 Paris, France*

E-mail: ivanez@apc.in2p3.fr, volpe@apc.in2p3.fr

Abstract: Neutrino being massive, they can decay. A heavier neutrino could decay into a lighter one and a massless scalar or pseudoscalar boson, such as the Majoron. Two-body non-radiative decay could occur in dense matter, such as in the inner dense regions of a core-collapse supernova. We first derive novel bounds on neutrino-Majoron couplings using the spectral distortions induced by neutrino non-radiative two-body decay in matter, and two-dimensional likelihood analyses of the 24 $\bar{\nu}_e$ events from SN1987A. We then explore the prospects of neutrino-Majoron couplings from a future galactic core-collapse supernova, leaving either a neutron star or a black-hole. To this aim, we use information from detailed one-dimensional supernova simulations. We consider the supernova neutrino signal associated with inverse-beta decay in the JUNO and upcoming Hyper-Kamiokande detectors, with neutrino-argon scattering in DUNE, or with coherent neutrino-nucleus scattering in the DARWIN experiment. In a full 3ν framework, based on the spectral distortions induced by neutrino decay in matter, we perform two-dimensional likelihood analyses and provide prospects for the limits on neutrino-Majoron couplings. Our results show that the observation of a future supernova will significantly improve on the current bounds, in particular from SN1987A and neutrinoless double-beta decay. Finally, we explore the impact of neutrino decay in matter on the diffuse supernova neutrino background formed by past supernova explosions. We show for the first time that the effects on black-hole contributions are important and modify the DSNB number of events by several tens of percent in Hyper-Kamiokande.

Keywords: neutrino properties, neutrino astronomy, supernova neutrinos

ArXiv ePrint: 2507.21845

*Corresponding author.

https://doi.org/10.1088/1475-7516/2026/02/069

JCAP02(2026)069

Contents

1 Introduction **1**

2 Theoretical framework **5**
- 2.1 The neutrino Hamiltonian 6
- 2.2 Neutrino non-radiative two-body decay in matter 8
- 2.3 Neutrino fluxes in presence of neutrino-Majoron interactions 9
- 2.4 Neutrino fluxes with decay: from the supernova core to the Earth 11

3 Supernova models and neutrino fluxes **13**
- 3.1 Supernova models 14
- 3.2 Results on the neutrino fluxes with decay 16

4 New bounds on neutrino-Majoron couplings from SN1987A **18**
- 4.1 Limits on (g, m) 19
- 4.2 Comparison of results with different models 22

5 Prospects on the neutrino-Majoron couplings from a future supernova **22**
- 5.1 Experiments 23
- 5.2 Predictions on the neutrino number of events 26
- 5.3 Prospects on the neutrino-Majoron couplings 28

6 Neutrino decay in matter and impact on the Diffuse Supernova Neutrino Background **31**
- 6.1 The DSNB flux 32
- 6.2 The DSNB model 33
- 6.3 Neutrino decay in matter and the DSNB: numerical results 34

7 Conclusions **38**

A Statistical analysis **40**

B Additional results **41**

1 Introduction

Neutrinos are unique elementary particles with mixing. Weakly interacting, they tell us about the interior of the Sun and of massive stars that undergo gravitational core-collapse. They are tightly linked to stellar nucleosynthesis processes and left an imprint on primordial nucleosynthesis, one second after the Big Bang. Milestone observations in astrophysics were the pioneering experiment of R. Davis on solar neutrinos [1] and the detection of SN1987A neutrino events, i.e., of the first neutrinos from the core-collapse of a massive star [2–4]. GW170817 was also unique, bringing the first measurement of gravitational waves concomitantly with a short gamma-ray burst and a kilonova [5]. A new window in

JCAP02(2026)069

neutrino astrophysics was opened with the detection of the first PeV neutrinos in the IceCube experiment [6] and, very recently, with the measurement of a cosmic neutrino event, with the highest energy ever observed, by the KM3NeT Collaboration [7].

After the breakthrough discovery of neutrino oscillations [8], solar, reactor, and accelerators have paved our knowledge of the neutrino oscillation parameters [9]. Still, many important open questions remain. Among the open questions is how neutrinos change flavor in dense environments. Indeed, neutral-current neutrino-neutrino interactions become sizable in such sites, and make neutrino propagation a non-linear many-body problem [10]. Moreover, collisions, shock wave, and turbulence effects also add to the complexity. In this context, important progress is being made to assess how neutrinos change flavor in dense environments (see [11–14] for reviews).

It is to be noted that the effects of the neutrino-neutrino interactions have made the object of intense investigations in the last two decades. While important progress was made in our understanding of their effects, because of the complexity of the problem, a definite assessment of its impact requires further extensive investigations [11–14]. Astrophysical and cosmological neutrinos provide complementary avenues to put tight constraints on unknown neutrino properties and new physics. Neutrinos are also tightly connected to dark matter searches in several ways and constitute a background for dark matter experiments, often referred to as the "neutrino floor". Interestingly, the PandaX-4T [15] and XENONnT [16] dark matter experiments found the first identification of ^{8}B solar neutrinos.

Core-collapse supernovae are among the most powerful neutrino sources. During their explosions, about 3×10^{53} erg of gravitational binding energy is taken away by neutrinos of all flavors in a ten-second burst. Core-collapse supernovae are rare events in our Galaxy. A combined analysis of different estimates of the core-collapse supernova rate gives a mean time of occurrence of 61^{+24}_{-14} years [17], Past supernovae in our Universe constitute the diffuse supernova neutrino background (DSNB) of all species, which is actively searched. A combined analysis of the ensemble of Super-Kamiokande data (SK) shows a hint at 1.8σ from the model-dependent analysis [18, 19]. Significance is now at the level of 2.3σ with the first results with the inclusion of Gadolinium, an idea first suggested in ref. [20] with the goal of suppressing backgrounds through better neutron tagging.

Unknown neutrino properties include neutrino non-radiative two-body decay. Core-collapse supernovae and cosmology have a unique sensitivity to long lifetime-to-mass ratios for this process (see figure 1 of ref. [21]). In particular, neutrino decay in vacuum or in matter into a massive Majoron, or a Majoron-like particle, was investigated based on CMB observations [22], using core-collapse supernovae as neutrino sources [23], considering the DSNB produced by past supernovae [24–27], or the 24 $\bar{\nu}_e$ events from SN1987A [21, 26, 28]. Ref. [29] investigated the impact of neutrino invisible decay in vacuum on solar, supernova and the DSNB neutrinos, giving prospects on the sensitivity on τ/m from future observations. Bounds on neutrino-Majoron couplings producing massive Majoron decays into neutrinos in supernovae were also derived from the absence of high-energy neutrinos [30–32]. Current limits on neutrino decay into a massive Majoron are summarized in figure 1. Note that bounds for massless Majorons (not shown) are provided by analyses based on the neutrino events from SN1987A [33–36].

JCAP02(2026)069

Unknown neutrino properties include neutrino non-radiative two-body decay into a massive or massless Majoron, or a Majoron-like particle. Core-collapse supernovae and cosmology have a unique sensitivity to long τ/m lifetime-to-mass ratios for this process (see figure 1 of ref. [21]). In particular, neutrino decay into a massive Majoron was investigated based on CMB observations [22] or using core-collapse supernovae as neutrino sources [23], or the 24 $\bar{\nu}_e$ events from SN1987A [21, 26, 28]. Bounds on neutrino-Majoron couplings producing massive Majoron decays into neutrinos in supernovae were also derived from the absence of high-energy neutrinos [30–32]. The impact of neutrino nonradiative decay in vacuum into a massless (pseudo)scalar boson was also investigated on the DSNB produced by past supernovae [24–27, 29]. Current limits on neutrino decay into a massive Majoron are summarized in figure 1. Note that bounds for massless Majorons (not shown) are provided by analyses based on the neutrino events from SN1987A [33–36].

Concerning the DSNB, ref. [21] provided the first investigation in a full 3ν framework including astrophysical uncertainties from the evolving core-collapse supernova rate. DSNB predictions in the absence and in the presence of decay are found to be degenerate for normal neutrino mass ordering, while for inverted mass ordering, the DSNB rates are strongly suppressed by neutrino decay. Ref. [27] provided the first Bayesian analysis combining different DSNB detection channels in SK, JUNO, DUNE, and Hyper-Kamiokande (HK) in a 3ν framework, with the goal of exploring the capability to discriminate DSNB predictions without and with neutrino non-radiative two-body decay. Such an analysis included the uncertainty in the evolving core-collapse supernova rate, and used neutrino fluxes from the Garching and Nakazato one-dimensional core-collapse supernova simulations. The results showed that, for the case of normal mass ordering, discriminating between the case with decay and without decay requires new avenues.

Numerous constraints on neutrino decay were also derived using the 24 $\bar{\nu}_e$ events from SN1987A, recorded in the Kamiokande [2], Irvine-Michigan-Brookhaven (IMB) [3] detectors and Baksan Scintillator Telescope (BST) [4]. These detectors were operating[1] when the supernova was observed, in the Large Magellanic Cloud, on the 27th of February 1987. Tight bounds were obtained concerning neutrino radiative decay [9]. Moreover, ref. [21] performed the first likelihood analysis of the SN1987A events, including the spectral distortion from non-radiative decay in vacuum. For inverted neutrino mass ordering, the analysis brought the lower bound of 2.4 (1.2) $\times 10^5$ eV/s at 68 % (90%) CL for the ν_2 and ν_1 neutrino mass eigenstates. This limit is tighter than previous ones, and competitive with cosmological ones (see e.g. [38]).

Neutrinos could also decay in matter. This possibility was studied in, e.g., refs. [33, 34, 39, 40]. Neutrino two-body decay can produce a pseudoscalar Goldstone boson, the Majoron, associated with total lepton number violation. Majorons were first introduced in a singlet model [41] and then in a triplet model [42], now excluded. In relation to SN1987A, limits on neutrino-Majoron couplings were discussed either using the cooling argument, or based on a deleptonization argument that exploits the ruled-out supernova prompt explosion mechanism [43], as well as using neutrino spectral distortions from neutrino decay [33, 34]. Ref. [35] refined the limits based on the cooling argument, whereas ref. [44] discussed decay

[1]Note that the Mont Blanc Liquid Scintillator Detector (LSD) recorded 5 events several hours before others [37].

JCAP02(2026)069

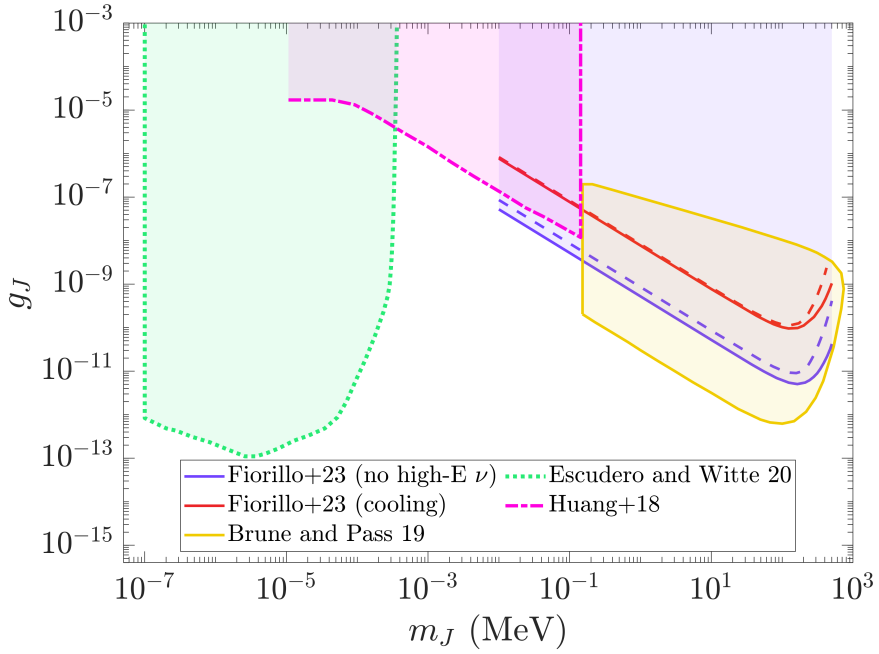

Figure 1. Current limits on the neutrino-Majoron coupling g_ϕ as a function of the Majoron mass m_ϕ. The bounds shown are obtained from: i) the absence of 100 MeV neutrinos from the decay of Majoron-like bosons (more stringent), or from the luminosity argument (less stringent) using a "hot" (solid line) and a "cold" (dashed line) supernova model [31]; ii) the luminosity argument applied to SN1987A neutrino events (closed contour) [23]; iii) CMB observations (dotted lines) [22]; iv) Big-bang nucleosynthesis (dot-dashed contour) [45].

rates of neutrino-Majoron decay in matter. Moreover, in our previous work ref. [36], we performed the first likelihood analysis of the spectral distortion of the SN1987A neutrino events due to neutrino-Majoron decay in matter. The analyses provided novel bounds on neutrino-Majoron couplings that go beyond the existing limits from SN1987A, and are competitive with those obtained from neutrinoless double-beta decay or several orders of magnitude better than the ones from lepton and meson decays.

In this manuscript, we present new bounds on neutrino-Majoron couplings, considering neutrino non-radiative two-body decay in matter, first considering SN1987A neutrino events, and then focusing on future observations of neutrinos from the next galactic core-collapse supernova. Following the theoretical framework developed in our previous work [36], we consider the impact on the supernova neutrino signal of neutrino two-body non-radiative decay in matter, into a massless (or almost massless) Majoron or Majoron-like particle. To this aim, we consider that the matter and decaying eigenstates coincide, and use detailed information from one-dimensional supernova simulations to calculate the neutrinosphere, transportsphere, and energysphere radii. These quantities are necessary to determine the impact of neutrino decay and the consequent neutrino spectral distortion. We first perform a likelihood analysis of the neutrino spectral distortions induced by neutrino decay, considering the 24 $\bar{\nu}_e$ events coming from SN1987A detected in the Kamiokande, IMB, and Baksan experiments, thus extending our previous work. Such analyses include the detailed response functions for each

JCAP02(2026)069

of the detectors. We then focus on a future galactic supernova, for which we consider the following two cases. i) A core-collapse supernova giving a neutron star (NS) for which we use the simulations from the Garching group [46, 47] that leave 1.36 $M_\odot$, 1.44 $M_\odot$, 1.62 $M_\odot$ with the DD2 or the SFHx neutron star equations-of-state (EOS). ii) A core-collapse supernova leaving a black-hole (BH) for which we employ Nakazato simulations for a 30 $M_\odot$ progenitor with the Lattimer-Swesty (L), the Shen (S), or the Togashi (T) EOS [48–50]. We present the impact of neutrino decay in matter on the core-collapse supernova neutrino fluxes, including also the well established Mikheev-Smirnov-Wolfenstein effect, and on the expected neutrino number of events in the JUNO, the upcoming HK, and the more distant future DUNE detector, as well as the DARWIN experiment. We then perform likelihood analyses of the spectral distortions of such events due to decay, considering both the signal in detectors individually and then combining them. We present novel bounds on neutrino-Majoron couplings and discuss how the limits improve on current ones and vary with the core-collapse supernova distance, in the Milky Way. Finally, we investigate the role of neutrino decay in matter on the DSNB, and explore its impact in the JUNO, HK, DUNE, and DARWIN detectors.

The manuscript is structured as follows. Section 2 introduces the 3ν formalism employed to study neutrino non-radiative two-body decay in matter. Section 3 presents the core-collapse supernova neutrino fluxes used from the Garching and Nakazato's one-dimensional simulations. Details are also given of the calculations of the neutrinospheres, the transportspheres, and the energyspheres necessary to compute the fluxes when neutrinos decay in matter. Section 4 discusses the likelihood analysis for the spectral distortion of SN1987A data in Kamiokande, IMB, and Baksan, and presents new results on the neutrino-Majoron bounds. Section 5 gives the expected number of events as well as the prospects on the neutrino-Majoron couplings using the neutrino signal from a future supernova in JUNO, HK, DUNE, and DARWIN. Section 6 presents the theoretical framework used for the DSNB, and our predictions for the expected DSNB number of events in the presence and in the absence of decay. Section 7 is a Conclusion. Finally, appendix A presents the statistical analysis we employ, and appendix B gives supplementary results.

2 Theoretical framework

Since neutrinos are massive particles, they could decay into a massless (or massive) scalar or pseudoscalar boson such as a Majoron, or a Majoron-like particle. Thus, while we will refer to Majorons, our analysis also holds for any massless (or almost massless) pseudoscalar boson.

Neutrino-Majoron interactions can be described generally by the following Lagrangian

$$\mathcal{L}_{\rm int} \propto \sum_{i,j} g_{ij} \bar{\nu}_i \gamma_5 \nu_j J \ , \tag{2.1}$$

in which ν_j (with $i, j = 1, 2, 3$) is the neutrino field and J the Majoron field. In the simplest Majoron models [51], the neutrino-Majoron coupling matrix g_{ij} is proportional to the neutrino mass matrix. Thus, the coupling matrix in the mass basis is diagonal and can be expressed as $g_{ij} \propto m_i \delta_{ij}$ with m_i the mass of the mass eigenstate i. Consequently, only one coupling is independent, and the remaining two are related to it by the values of the squared-mass

JCAP02(2026)069

differences measured in oscillation experiments. In our study, we will consider the theoretical framework of three active neutrino flavors.

It is to be noted that the proportionality of the coupling matrix to the mass matrix implies a suppression of the decay $\nu_h \to \nu_l + J$ in vacuum, from a heavier ν_h to a lighter ν_l neutrino. Interestingly, in matter, the interactions of neutrinos with the particles in the medium induce effective neutrino masses breaking this proportionality [52]. Thus, off-diagonal terms g_{ij} $(i \neq j)$ appear in the coupling matrix, allowing new interaction channels that can enhance neutrino decay in matter to Majorons.

Thus, in our analysis, there is only one independent coupling. For the case of normal neutrino mass ordering, g_{11} and m_1 will be our fit parameters, with the other two couplings g_{22} and g_{33} determined following the relations

$$g_{22} = g_{11}\sqrt{1 + \frac{\Delta m^2_{21}}{m_1^2}}, \quad g_{33} = g_{11}\sqrt{1 + \frac{\Delta m^2_{31}}{m_1^2}}\,. \tag{2.2}$$

Similarly, in the case of inverted neutrino mass ordering, g_{33} and m_3 will be our fit parameters, with g_{11} and g_{22} derived through analogous expressions

$$g_{11} = g_{33}\sqrt{1 + \frac{|\Delta m^2_{31}|}{m_3^2}}, \quad g_{22} = g_{33}\sqrt{1 + \frac{|\Delta m^2_{32}|}{m_3^2}}\,. \tag{2.3}$$

2.1 The neutrino Hamiltonian

We introduce here the 3ν theoretical framework describing neutrino evolution in matter. The Hamiltonian describing neutrino propagation in a core-collapse supernova, including neutrino decay, can be expressed as

$$H = H_0 + H_{\rm matter} + H_{\rm int}\,, \tag{2.4}$$

the first is the vacuum term, the second accounts for the interactions with the particles in the medium, and the last implements neutrino-Majoron interactions eq. (2.1). In dense environments, such as a core-collapse supernova, the neutrino-neutrino interactions, shock wave effects, and turbulence might also influence the neutrino spectra (see, for example, [11–14] for reviews). In particular, the neutral-current neutrino-neutrino interactions make neutrino evolution a complex weakly interacting many-body problem, which is still under active investigation. Indeed the solution of the full problem is numerically very challenging, since its solution would require solving neutrino quantum kinetic equations that depend on time, on the neutrino position and momentum (the phase space is thus seven dimensional) with sizable $\nu\nu$ interactions making it a nonlinear many-body problem. Therefore, in the present analysis, we only consider neutrino-matter contributions responsible for the well-established Mikheev-Smirnov-Wolfenstein effect [53, 54].

The first contribution to the neutrino Hamiltonian is responsible for the well-established phenomenon of neutrino vacuum oscillations. In the flavor basis, it reads

$$H_0 = U H_{\rm vac} U^\dagger\,, \tag{2.5}$$

JCAP02(2026)069

with $H_{\rm vac} = diag(E_i)$ $(i = 1, 3)$ being the propagation Hamiltonian of the mass eigenstates, and E_i the corresponding neutrino energies. Since neutrinos are ultrarelativistic (in the equal momentum approximation), the elements of the vacuum Hamiltonian read

$$H_{vac,ij} = \left[E + \frac{m_i^2}{2E}\right]\delta_{ij}\,, \tag{2.6}$$

where $E = |\vec{p}|$, with $\vec{p}$ the neutrino momentum and δ_{ij} the Kronecker delta.

The unitary matrix U ($U^\dagger = U^{-1}$) is the Pontecorvo-Maki-Nakagawa-Sakata (PMNS) matrix relating the mass and flavor bases

$$|\nu_\alpha\rangle = U^*_{\alpha i}|\nu_i\rangle\,, \tag{2.7}$$

(a summation on the i index is subtended). For 3ν flavors, the PMNS matrix is parametrized as[2] [9]

$$U = \begin{pmatrix} c_{12}c_{13} & s_{12}c_{13} & s_{13}e^{-i\delta} \\ -s_{12}c_{23} - c_{12}s_{13}s_{23}e^{i\delta} & c_{12}c_{23} - s_{12}s_{13}s_{23}e^{i\delta} & c_{13}s_{23} \\ s_{12}s_{23} - c_{12}s_{13}c_{23}e^{i\delta} & -c_{12}s_{23} - s_{12}s_{13}c_{23}e^{i\delta} & c_{13}c_{23} \end{pmatrix}\,, \tag{2.8}$$

with $c_{ij} = \cos\theta_{ij}$, $s_{ij} = \sin\theta_{ij}$ $(i, j = 1, 3)$ and δ the Dirac CP violating phase that we set to zero in our work.

As neutrinos propagate in the supernova layers, they interact with the electrons, protons, and neutrons composing the medium. Electron neutrinos ν_e and antineutrinos $\bar{\nu}_e$ interact through both charged-current (CC) and neutral-current (NC) interactions, whereas non-electron neutrinos ν_x and antineutrinos $\bar{\nu}_x$ $(x = \mu,\ \tau)$ mostly experience NC interactions.[3] The corresponding potentials, in the mean-field approximation, are given by

$$\begin{aligned} V_{\rm CC} &= \sqrt{2}G_F n_B(Y_e + Y_{\nu_e}), \\ V_{\rm NC} &= \sqrt{2}G_F n_B\left(-\frac{1}{2}Y_n + Y_{\nu_e}\right), \end{aligned} \tag{2.9}$$

with G_F the Fermi constant, n_B the baryon density, and $Y_i = (n_i - \bar{n}_i)/n_B$ the particle number fraction[4] with $i = e$ (electrons), ν_e, and n (neutrons). For antineutrinos, these potentials have opposite signs. Thus, in the flavor basis, the mean-field neutrino-matter Hamiltonian is

$$V_{\alpha\beta} = \begin{pmatrix} V_{\rm CC} + V_{\rm NC} & 0 & 0 \\ 0 & V_{\rm NC} & 0 \\ 0 & 0 & V_{\rm NC} \end{pmatrix}\,. \tag{2.10}$$

Putting the different contributions together, the neutrino Hamiltonian eq. (2.4) becomes

$$H = E\mathbb{I} + \frac{1}{2E}U\mathrm{M}^2U^\dagger + V_{\alpha\beta}\,, \tag{2.11}$$

where $\mathbb{I}$ is the identity matrix.

[2]Note that we do not consider here the two Majorana phases that are not relevant in our analyses.

[3]We neglect here the presence of a finite density of muons in the core-collapse supernova core, that breaks the degeneracy between muon and tau neutrinos (and antineutrinos) [55].

[4]Note that in our computations we set Y_ν =0.

JCAP02(2026)069

2.2 Neutrino non-radiative two-body decay in matter

In our treatment of neutrino two-body non-radiative decay in matter, we extend the framework of refs. [33, 34]. To discuss the effect of neutrino decay in matter, we use the matter basis that instantaneously diagonalizes the neutrino Hamiltonian (2.4), including the vacuum and the matter contributions (only), through the following transformation

$$\tilde{H} = \tilde{U} H \tilde{U}^\dagger \,, \tag{2.12}$$

where $\tilde{U}$ is the mixing matrix in matter, relating the flavor and matter bases

$$|\nu_\alpha\rangle = \tilde{U}_{\alpha i} |\tilde{\nu}_i\rangle \,, \tag{2.13}$$

Note that $\tilde{U}$ depends on the helicity of neutrinos, i.e. negative (positive) for neutrinos (antineutrinos) and on the neutrino mass ordering.

For illustration purposes, let us discuss the case of 2ν flavors. In this case, the matrices $U = R(\theta)$ and $\tilde{U} = R(\tilde{\theta})$ are rotation matrices parametrized by the θ and $\tilde{\theta}$ angles. The diagonalization of H eq. (2.12) requires

$$\tan 2\tilde{\theta} = \frac{\sin 2\theta}{\cos 2\theta - 2EV_{\rm CC}/\Delta m^2} \,, \tag{2.14}$$

with $\Delta m^2 = m_2^2 - m_1^2$ the squared-mass difference. At very high densities, $|V_{\rm CC}| \to \infty$, the matter mixing angle is "suppressed", i.e. $\tilde{\theta} \to \pi/2$ (0) for neutrinos (antineutrinos), so that the matter and the flavor eigenstates essentially coincide.

For 3ν flavors, the mixing matrix in matter can be parametrized as

$$\tilde{U} = \tilde{U}_{12} \tilde{U}_{13} \tilde{U}_{23}, \tag{2.15}$$

where $\tilde{U}_{ij} = \tilde{U}_{ij}(\tilde{\theta}_{ij})$ are rotation matrices in the i-j plane by an angle $\tilde{\theta}_{ij}$ (we fixed $\delta = 0°$). Since the neutrino mass ordering can be normal or inverted, because the sign of Δm^2_{31} is unknown, the sign of the second term in the denominator of eq. (2.14) can be positive or negative, thus affecting the value of $\tilde{\theta}_{13}$. Table 1 shows the correspondence, at high matter densities, between the matter and flavor eigenstates, considering both normal and inverted mass ordering.

In general, the coupling matrix in the matter basis is related to the one in the flavor basis through

$$\tilde{g}_{ij}^{h_i \to h_j} = \tilde{U}_{i\alpha}^{(h_i)\dagger} g_{\alpha\beta} \tilde{U}_{\beta j}^{(h_j)}, \tag{2.16}$$

where we added the notation $h_{i,j}$ here to indicate the neutrino helicity. At high densities, the coupling matrix in the matter basis can be approximated by the one in the rotated flavor basis [33, 34]:

$$\tilde{g}_{ij} \to U_{23}(\theta_{23}) g_{\alpha\beta} U_{23}(-\theta_{23}) = g_{\alpha'\beta'} \,. \tag{2.17}$$

From eqs. (2.16)–(2.17), we observe that the coupling matrix in matter is no longer diagonal and that, deep in the stellar interior, a Majoron-like particle couples to flavor

JCAP02(2026)069

	$\tilde{\nu}_1^{(-)}$	$\tilde{\nu}_2^{(-)}$	$\tilde{\nu}_3^{(-)}$	$\tilde{\nu}_1^{(+)}$	$\tilde{\nu}_2^{(+)}$	$\tilde{\nu}_3^{(+)}$
NO	$\nu_{\mu'}$	$\nu_{\tau'}$	ν_e	$\bar{\nu}_e$	$\bar{\nu}_{\mu'}$	$\bar{\nu}_{\tau'}$
IO	$\nu_{\mu'}$	ν_e	$\nu_{\tau'}$	$\bar{\nu}_{\tau'}$	$\bar{\nu}_{\mu'}$	$\bar{\nu}_e$

Table 1. Correspondence between the matter and the flavor eigenstates in a 3ν flavor framework, for both normal (NO) and inverted (IO) neutrino mass orderings. The superscript in the matter eigenstates indicates the helicity, namely $(-)$ for neutrinos and $(+)$ for antineutrinos. The prime indicates a rotated basis in the ν_μ-ν_τ subspace.

neutrino eigenstates. In the relativistic approximation, only helicity-flipping neutrino decays are allowed with the total decay rate of the process $\nu_\alpha^{(\pm)} \to \nu_\beta^{(\mp)} + J$ given by [33, 52]

$$\Gamma_{\alpha\beta} = \frac{g_{\alpha\beta}^2}{16\pi} \Delta V_{\alpha\beta} \,, \tag{2.18}$$

with $\alpha, \beta = e, \mu', \tau'$ (the prime indicates the rotated basis). This process is only allowed if

$$\Delta V_{\alpha\beta} = V_\alpha - V_\beta > 0 \,. \tag{2.19}$$

The energy distribution of the daughter neutrinos is given by the following expression [56]

$$\psi(E_\alpha, E_\beta) = \frac{2}{E_\alpha} \left(1 - \frac{E_\beta}{E_\alpha}\right) , \tag{2.20}$$

where E_α and E_β correspond to the energies of the initial and final neutrino, respectively.

2.3 Neutrino fluxes in presence of neutrino-Majoron interactions

After being produced in the supernova core, neutrinos can undergo decay in matter when the condition (2.19) is fulfilled. To treat the influence of decay, in contrast with ref. [33] we employ a theoretical framework that implements the time dependence of the neutrino emission in the core-collapse supernova. Interestingly, the computation of the impact of neutrino decay includes a term in the survival probability, first pointed out in ref. [33] (see eq. (2.22)) that involves an effective neutrino velocity and dominates over the constant term previously considered. The early work [33] evaluated its contribution by assuming time-independent density profiles using inputs from ref. [57] (at time $t = 6$ s). In our framework, we perform a detailed calculation of this term, of the associated mean-free paths for the different microscopic processes that influence the neutrino species.

In the models we employ and the relevant radii, the condition (2.19) is fulfilled for $\bar{\nu}_e$ only (and not for ν_e). Therefore, neutrinos will be treated as stable. The survival probability of $\bar{\nu}_e$ with energy E_ν emitted at the neutrinosphere is given by [33]

$$N_{\bar{\nu}_e}(E_\nu) = \exp\left\{ \int_{R_{\rm NS}}^{\infty} dr' \; \Gamma_{\bar{\nu}_e}(r') \right\} . \tag{2.21}$$

For $\bar{\nu}_x$ emitted at the energysphere, the survival probability reads

$$N_{\bar{\nu}_x}(E_\nu) = \exp\left\{ - \int_{R_{\rm ES}}^{R_{\rm TS}} \frac{dr'}{v(E_\nu, r')} \Gamma_{\bar{\nu}_x}(r') - \int_{R_{\rm TS}}^{\infty} dr' \; \Gamma_{\bar{\nu}_x}(r') \right\} . \tag{2.22}$$

JCAP02(2026)069

In these expressions, r' is the radial distance to the core-collapse supernova core. The term $\Gamma_{\bar{\nu}_\alpha} = \sum_{\beta=e,\mu,\tau} \Gamma_{\alpha\beta}$ represents the total decay rate. In eq. (2.22), the first integral inside the exponential accounts for the decay occurring between the energysphere $R_{\rm ES}$ and the transportsphere $R_{\rm TS}$. As we will discuss, their values averaged over energy will be employed in our calculations. In this region, $\bar{\nu}_x$ are no longer in thermal equilibrium, but they remain trapped and diffuse outwards with an effective velocity given by $v(E_\nu, r) = \lambda(E_\nu, r)/(R_{\rm TS} - R_{\rm ES})$ where λ is the mean free-path. The second term in the exponential represents the decay once $\bar{\nu}_x$ start free-streaming. In contrast, in eq. (2.21), there is only one term inside the exponential. In this case, $\bar{\nu}_e$ fall out of equilibrium and start free-streaming at the same point. Thus, only decay occurring beyond the neutrinosphere $R_{\rm NS}$ affects the spectrum.

Energysphere, transportsphere, and neutrinosphere. The neutrino flux suppression due to neutrino decay in matter requires the computation of the neutrinosphere for $\bar{\nu}_e$ (2.21), the energysphere and the transportsphere for $\bar{\nu}_x$ and ν_x (2.22). The main processes that keep ν_e and $\bar{\nu}_e$ in thermal equilibrium are beta processes [58]:

$$\nu_e + n \leftrightarrow p + e^- \,, \quad \bar{\nu}_e + p \leftrightarrow n + e^+ \,. \tag{2.23}$$

These processes freeze out at a region called the neutrinosphere, where ν_e and $\bar{\nu}_e$ fall out of thermal equilibrium and start free streaming. The radius $r_{\rm NS}$ of the neutrinosphere is defined as the energy-dependent location where the optical depth is equal to 2/3, i.e.,

$$\tau(r_{\rm NS}) = \int_{r_{\rm NS}}^{\infty} dr \lambda_\beta^{-1}(r) = \frac{2}{3} \,, \tag{2.24}$$

where $\lambda_\beta^{-1}(r)$ is the inverse mean free-path[5] of neutrinos associated to the beta processes eq. (2.23). We remind that the mean free path of a particle that interacts through several processes is calculated as

$$\lambda^{-1}(r, E) = \sum_i \lambda_i^{-1}(r, E) = \sum_i n_i(r) \sigma_i(E) \,, \tag{2.25}$$

where the index i runs over all the processes, the cross section of these processes is denoted by σ_i, and n_i indicates the target number.

Regarding the non-electronic flavors, neutral-current collisions on nucleons N

$$\nu + N \leftrightarrow \nu + N \,, \tag{2.26}$$

are the main processes through which ν_x and $\bar{\nu}_x$ interact with the medium [58]. The energy exchange in this process is inefficient due to the large mass of the nucleons ($m_N \sim 940\,\text{MeV}$) compared to the neutrino energies ($E_\nu \sim 10\,\text{MeV}$). Consequently, other processes are instead responsible for keeping ν_x and $\bar{\nu}_x$ in thermal equilibrium: nucleon-nucleon bremsstrahlung and leptonic processes, respectively

$$N + N \leftrightarrow N + N + \nu + \bar{\nu} \,, \quad e^+ + e^- \leftrightarrow \nu + \bar{\nu} \,, \quad \nu + e \leftrightarrow \nu + e \,. \tag{2.27}$$

[5] Not to overburden the text, the explicit dependence on the neutrino energy in eq. (2.24) (coming from the energy-dependence of the mean free-path) was dropped.

JCAP02(2026)069

Non-electronic neutrinos and antineutrinos are kept in thermal equilibrium until these interactions freeze out at the energysphere. The radius of the energysphere $r_{\rm ES}$ is found using the thermal optical depth [58, 59]:

$$\tau(r_{\rm ES}) = \int_{r_{\rm ES}}^{\infty} dr \sqrt{\lambda_E^{-1}(r)\left[\lambda_T^{-1}(r) + \lambda_E^{-1}(r)\right]} = \frac{2}{3}\,. \tag{2.28}$$

In this expression, λ_E^{-1} and λ_T^{-1} denote the "energy" and "transport" inverse mean free paths[6] For the calculation of the "energy" mean free path, we consider only nucleon bremsstrahlung, $\lambda_E = \lambda_{\rm brem}$, which dominates over the leptonic processes [58]. For the "transport" mean free path, we consider NC collisions on nucleons, $\lambda_T^{-1} = \lambda_{\nu p}^{-1} + \lambda_{\nu n}^{-1}$.

Finally, the NC interactions of neutrinos with nucleons keep ν_x and $\bar{\nu}_x$ trapped up to the transportsphere. The radius of the energy-dependent transportsphere $r_{\rm TS}$ can be obtained using the following expression

$$\tau(r_{\rm TS}) = \int_{r_{\rm TS}}^{\infty} dr \lambda_T^{-1}(r) = \frac{2}{3}\,. \tag{2.29}$$

2.4 Neutrino fluxes with decay: from the supernova core to the Earth

In order to calculate the core-collapse supernova neutrino fluxes[7] including neutrino decay, one needs $\phi^0_{\nu_\alpha}(E_\nu, t)$, namely the flux of neutrinos ν_α with energy E_ν at a post-bounce time t produced in the deep regions of the supernova core, before decoupling.

Supernova neutrino fluxes before decay. Since we consider the possibility that the next galactic core-collapse supernova leaves either a NS or a BH, we use two sets of simulations from the literature, one from the Garching group for the NS case, and one from Nakazato's work for the BH case. The inputs for the neutrino fluxes for the two sets of core-collapse supernova simulations differ.

NS case. For the Garching simulations [46, 47], the neutrino fluxes are well accounted by the usual power-law distribution [60], namely

$$\phi^0_{\nu_\alpha}(E_\nu, t) = \frac{L_\nu(t)}{\langle E_\nu(t)\rangle}\varphi_{\nu_\alpha}(E_\nu, t)\,, \tag{2.30}$$

where $L_\nu(t)$ and $\langle E_\nu(t)\rangle$ indicate the neutrino luminosity and average energy, respectively. The neutrino energy distribution is given by

$$\varphi_{\nu_\alpha}(E_\nu, t) = \frac{1}{\langle E_\nu(t)\rangle}\frac{[\alpha(t)+1]^{\alpha(t)+1}}{\Gamma\left(\alpha(t)+1\right)}\left(\frac{E_\nu}{\langle E_\nu(t)\rangle}\right)^{\alpha(t)} \exp\left\{-\frac{[1+\alpha(t)]\,E_\nu}{\langle E_\nu(t)\rangle}\right\}. \tag{2.31}$$

In this expression, $\alpha(t)$ represents the pinching parameter related to the first and second moments of the energy through the relation

$$\alpha(t) = \frac{\langle E_\nu(t)^2\rangle - 2\langle E_\nu(t)\rangle^2}{\langle E_\nu(t)\rangle^2 - \langle E_\nu(t)^2\rangle}\,. \tag{2.32}$$

[6] It is to be noted that if neutrinos propagate in a medium where neutrinos interact either through a iso-energetic scattering with λ_T and a scattering process with energy-dependence that changes the energy significantly λ_E, one can introduce an effective mean free-path taking into account the random walk of the neutrinos is given by $\lambda_{\rm eff} = (\lambda_E \lambda_T)^{1/2}$. These lead to the expression for the optical depth (2.28) [58, 59].

[7] Note that we omit the dependence of the core-collapse supernova neutrino fluxes on the progenitor mass, not to overburden the text.

JCAP02(2026)069

BH case. For Nakazato's simulations [48, 49, 61], we directly use the numerical output and perform a log-linear interpolation of the data. An example of the numerical fit is shown in figure 17 of ref. [27].

Supernova neutrino fluxes with decay. In order to implement the time-dependence, our theoretical framework employs time-dependent information from detailed supernova simulations. To this aim, the core-collapse supernova evolution was split into six intervals to optimize the computation. We chose a representative time point for each interval $\tilde{t}_i \in [t_{i-1}, t_i]$ and calculated the survival probabilities eqs. (2.21)–(2.22) at that time $N^i_{\bar{\nu}_\alpha}(E_\nu) = N_{\bar{\nu}_\alpha}(E_\nu, \tilde{t}_i)$. We then applied this survival probability to the fluxes in the corresponding time ranges. Namely, the antineutrino fluxes after decay at time $t \in [t_{i-1}, t_i]$ $(i = 1, \ldots, 6)$ become

$$\phi^d_{\bar{\nu}_\alpha}(E_\nu, t) = N^i_{\bar{\nu}_\alpha}(E_\nu)\phi^0_{\bar{\nu}_\alpha}(E_\nu, t)\,. \tag{2.33}$$

where the first factor is given by (2.21)–(2.22).

If neutrinos can decay, the neutrino fluxes as a function of time, when neutrinos start free-streaming, can be expressed as follows

$$\phi^d_{\nu_\alpha}(E_\nu, t) = \phi^0_{\nu_\alpha}(E_\nu, t) + \phi^\Delta_{\nu_\alpha}(E_\nu, t)\,. \tag{2.34}$$

Here $\phi^\Delta_{\nu_\alpha}(E_\nu, t)$ is the contribution to the neutrino flux from the antineutrinos that underwent decay. The latter can be determined using the expression

$$\phi^\Delta_{\nu_\alpha}(E_\nu, t) = \int_{E_\nu}^{\infty} dE'_\nu \psi(E'_\nu, E_\nu) \sum_{\beta=e,\mu,\tau} \left[1 - N^i_{\bar{\nu}_\beta \to \nu_\alpha}(E'_\nu)\right] \phi^0_{\bar{\nu}_\beta}(E_\nu, t)\,. \tag{2.35}$$

The factor $\psi(E'_\nu, E_\nu)$ represents the energy distribution of the daughter neutrino eq. (2.20), and $N^i_{\bar{\nu}_\beta \to \nu_\alpha}$ are the partial survival probabilities of $\bar{\nu}_\beta$ to ν_α in the i time interval. We remind that only antineutrinos satisfy the condition for decay in matter given by the relation (2.19).

In order to verify that our numerical results do not depend on the procedure we use, we checked that they do not depend on the representative points $\tilde{t}_i$ in each interval, and we increased the number of intervals from six to ten. While two intervals were sufficient for the accretion phase, the cooling phase required at least three intervals to achieve an accurate representation. It is to be noted that we also checked the consistency of our results with those of ref. [33] by considering a single time interval and using the core-collapse supernova profiles from the Wilson model [57], and obtained good agreement.

It is to be noted that the neutrino-neutrino interaction can potentially modify the neutrino flavor spectra and neutrino evolution close to the neutrinosphere and far from it. However, in spite of almost twenty years investigations, the study of the neutrino-neutrino interaction, a non-linear many-body problem, keeps being a rapidly evolving domain where new aspects keep being uncovered and also the treatments of neutrino-neutrino interaction debated.[8] Clearly,

[8]For fast modes e.g. that can occur close to the neutrinosphere on very short (subgrid) scales, studies are searching possible steady-state solutions considering boxes of a few km size. It appears that the use of boxes without boundary do not lead to any steady-state solution (see e.g. [62]). Concerning slow modes, previous investigations showed they occur far from the neutrinosphere [11], whereas recently ref. [63] pointed out that they might be the first to appear and impact the conditions for the fast instabilities. Furthermore new approaches are also emerging such as in ref. [64] that treats collective modes induced by the neutrino-neutrino interaction as flavor waves, or flavomons, and have not yet been applied to realistic situations.

JCAP02(2026)069

a definite assessment on the role of the neutrino-neutrino interaction will require future work. For these reasons, the present manuscript focuses on neutrino decay in matter considering the established MSW effect. The inclusion of neutrino-neutrino interaction effects is beyond the purpose of the present manuscript and will make the object of future investigations.

Once the neutrinos reach the MSW region, their fluxes are modified by neutrino-matter interaction. Thus, depending on the sign of the squared mass differences $\Delta m^2_{31} = m^2_3 - m^2_1$ (that still remains unknown), the neutrino yields at the supernova surface become[9]

$$\begin{aligned} &\phi_{\nu_1} = \phi^d_{\nu_x} \quad &&\phi_{\nu_2} = \phi^d_{\nu_x} \quad &&\phi_{\nu_3} = \phi^0_{\nu_e} \quad &&\text{(NO)}\,, \\ &\phi_{\nu_1} = \phi^d_{\nu_x} \quad &&\phi_{\nu_2} = \phi^0_{\nu_e} \quad &&\phi_{\nu_3} = \phi^d_{\nu_x} \quad &&\text{(IO)}\,, \end{aligned} \tag{2.36}$$

and the antineutrino yields are

$$\begin{aligned} &\phi_{\bar{\nu}_1} = \phi^d_{\bar{\nu}_e} \quad &&\phi_{\bar{\nu}_2} = \phi^d_{\nu_x} \quad &&\phi_{\bar{\nu}_3} = \phi^d_{\nu_x} \quad &&\text{(NO)}\,, \\ &\phi_{\bar{\nu}_1} = \phi^d_{\nu_x} \quad &&\phi_{\bar{\nu}_2} = \phi^d_{\nu_x} \quad &&\phi_{\bar{\nu}_3} = \phi^d_{\bar{\nu}_e} \quad &&\text{(IO)}\,, \end{aligned} \tag{2.37}$$

with NO standing for normal (i.e. $\Delta m^2_{31} > 0$) and IO for inverted (i.e. $\Delta m^2_{31} < 0$) ν mass ordering.

Finally, neutrinos propagate in vacuum from the core-collapse supernova surface to the Earth. In a detector on Earth, the fluxes in the flavor basis are related to the ones in the mass basis through the relation

$$\phi_{\nu_\alpha}(E_\nu, t) = \frac{1}{4\pi L^2} \sum_{i=1,3} |U_{\alpha i}|^2 \phi_{\nu_i}(E_\nu, t)\,, \tag{2.38}$$

where L is the core-collapse supernova distance. Here, $U_{\alpha i}$ are the elements of the PMNS matrix.

3 Supernova models and neutrino fluxes

The evolution of a core-collapse supernova during the explosion and the corresponding neutrino emission can be divided into three main phases.

At early times, as the shock breaks out from the neutrinosphere, large amounts of ν_e are produced through the neutronization of the core, leading to the so-called neutronization burst (figures 2 and 3, left panels). During this phase, the ν_e luminosity is very high, around $L_{\nu_e} \sim 10^{53}$ erg/s, though it lasts only about 50 ms. Following this, matter keeps falling and accreting the core in what is called the accretion phase (figures 2 and 3, middle panels), which lasts up to several hundred ms. In this phase, neutrinos and antineutrinos of all flavors are emitted with luminosities of $\sim 10^{52}$ erg/s (or higher if a BH is formed). The shock wave stalls at this stage, and a core-collapse supernova explosion is only possible if some mechanism revives the shock.

Currently, the shock revival is thought to happen via neutrino energy deposition, combined with neutrino-induced convection and turbulence, in the so-called *delayed neutrino heating*

[9] Note that here we neglect the explicit dependence of the neutrino fluxes on energy and time, not to overburden the text.

JCAP02(2026)069

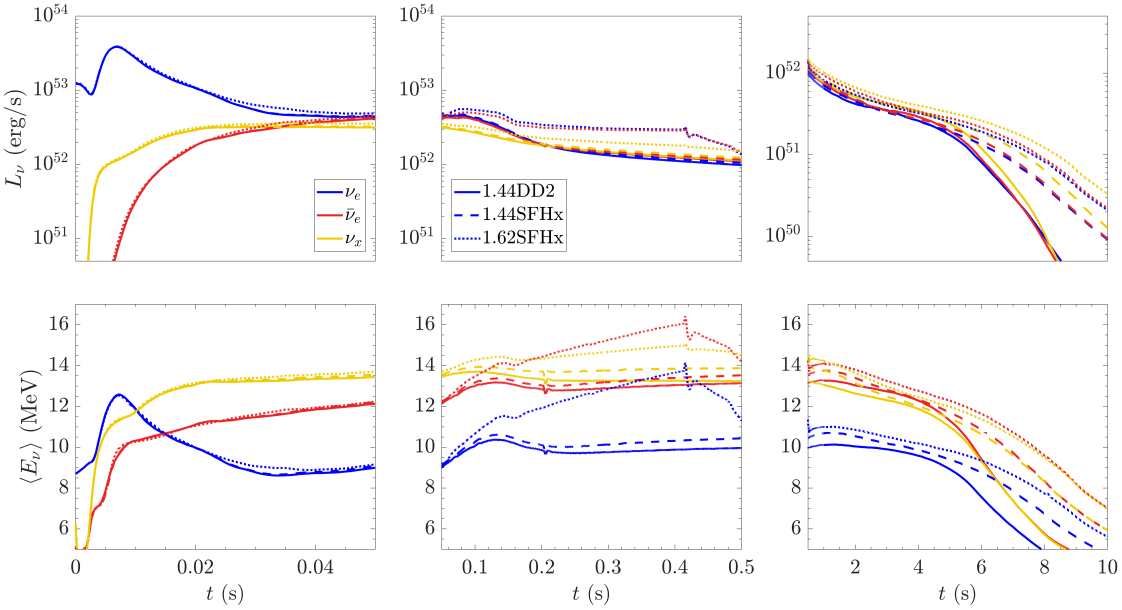

Figure 2. *NS case:* parameters defining the neutrino fluxes, as a function of time, for a core-collapse supernova at 10 kpc leaving a NS. The three phases of the core-collapse supernova explosion are shown, namely the neutronization burst (left), the accretion (middle), and the cooling phase of the newly born neutron star (right figures). As a function of time, the figures present the neutrino luminosity or the neutrino average energies. The curves correspond to the models 1.44 DD2 (solid lines), 1.44 SFHx (dashed lines), and 1.62 SFHx (dotted lines) from one-dimensional simulations of the Garching group. For each model the results are for ν_e (blue), $\bar{\nu}_e$ (red), and ν_x (yellow lines). (With courtesy from [46, 47].)

mechanism first introduced by Bethe and Wilson [65]. Finally, the last stage of the neutrino emission during the death of a massive star is the cooling of the newly formed proto-neutron star (if the core-collapse supernova does not leave a black-hole). So, the luminosity significantly decreases, and neutrinos are emitted with a quasi-thermal spectrum and almost luminosity equipartition across flavors (figure 2, right panels). This last phase lasts for several seconds up to ~ 10 s if a NS is formed. Interestingly, if the core-collapse supernova is close enough, one could also detect the pre-supernova neutrinos from the last few days of the Si-burning phase preceding the core-collapse [66], and also measure the late-time cooling of the proto-neutron star that would be informative on the neutron star equation-of-state (EOS), the fate of the core-collapse supernova, and possible non-standard cooling mechanisms [67].

3.1 Supernova models

Our investigation considers that the core-collapse supernova leaves either a NS or a BH. To this aim, we exploit the outcome of detailed one-dimensional core-collapse supernova simulations either from the Garching group for the NS case [46, 47], or from Nakazato for the BH case [48, 49, 61]. Note that Garching simulations account well for SN1987A observations, in particular for the time-integrated fluxes, the cumulative energy and event distribution of the 24 $\bar{\nu}_e$, except for the late neutrino events.

JCAP02(2026)069

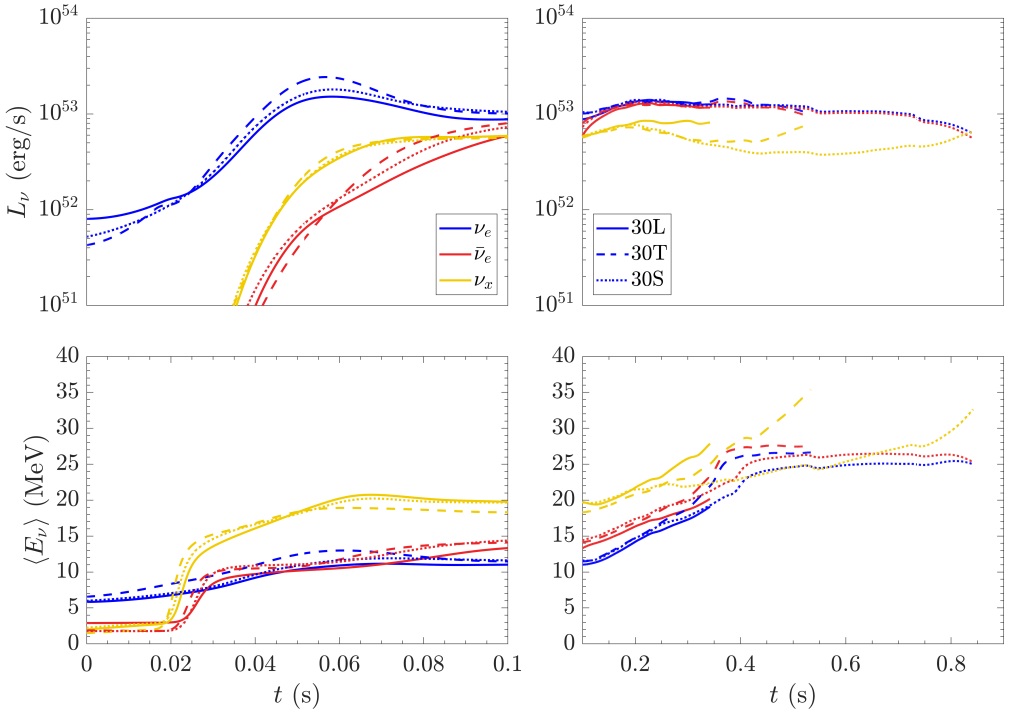

Figure 3. *BH case:* parameters defining the neutrino fluxes, as a function of time, for a core-collapse supernova at 10 kpc leaving a BH. The figures show the neutrino luminosity and the neutrino average energies, as functions of time, for the 30 $M_\odot$, with metallicity $Z = 0.004$ and the LS220 (L), the Shen (S) or the Togashi (T) EOS, from Nakazato's simulations. (With courtesy from [48, 49, 61].)

In contrast with ref. [33], in our framework, the neutrino emission is time-dependent and the transportspheres, the energyspheres, and the neutrinospheres are determined from microscopic processes, namely nucleon-nucleon bremsstrahlung, neutrino-nucleon NC interaction, and inverse-beta decay. Thus, to compute the neutrino decay rates in matter eq. (2.18) and the survival probabilities for $\bar{\nu}_e$ eq. (2.21) and ν_x eq. (2.22) we use the neutrino fluxes, the matter densities $\rho(t, r)$ as a function of position and time, and the electron fraction $Y_e(t, r)$ from detailed core-collapse supernova simulations.

Figure 2 illustrates the evolution of two of the parameters that characterize the core-collapse supernova neutrino fluxes, i.e., the luminosity, the average energy for the different neutrino flavors. The results correspond to the two sets of supernova simulation results used in our study. For the NS case we considered the supernova simulation inputs corresponding to the two neutron star masses 1.44 $M_\odot$ and 1.62 $M_\odot$ with either the SFHx [68] or the DD2 [69] NS EOS. On the other hand, figure 3 shows the evolution of the neutrino luminosities and average energies for the three neutrino species for the BH that corresponds to a 30 $M_\odot$ progenitor, with metallicity $Z = 0.004$ and three different EOS, namely the LS220 (L), the Shen (S), or the Togashi (T) one [48, 49, 61].

JCAP02(2026)069

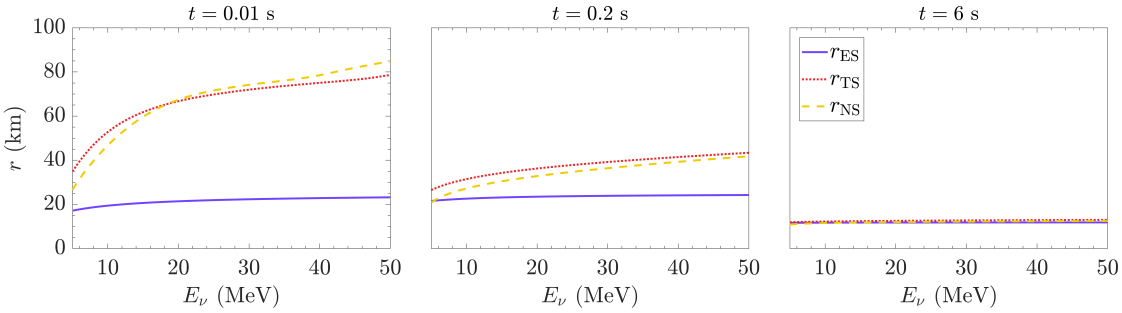

Figure 4. The figure shows examples of the results for the neutrinosphere, the transportsphere, and the energysphere at three different time snapshots, during the neutronization burst, the accretion phase, and the cooling of the newly formed proto-neutron star. The results correspond to the 1.44SFHx model for the NS case.

3.2 Results on the neutrino fluxes with decay

It is interesting to look at the impact of neutrino decay in matter on the neutrino fluxes for different values of the neutrino-Majoron couplings. For the computation of the neutrino fluxes eq. (2.38) we use the following values of the neutrino mixing angles, $\sin^2\theta_{12} = 0.307$, $\sin^2\theta_{23} = 0.547(0.534)$, and $\sin^2\theta_{13} = 0.02$ for normal (inverted) neutrino mass ordering [9].

In figure 4, we give three examples of the energy-dependent energyspheres and transportspheres for the three phases of neutronization burst, accretion phase, and cooling of the newly born proton-neutron star for information. As for the averages of such radii over energy one gets $R_{\rm ES} = 21.9$ km, $R_{\rm TS} = 69.2$ km, and $R_{\rm NS} = 70.5$ km for $t = 0.01$ s; $R_{\rm ES} = 23.7$ km, $R_{\rm TS} = 38.3$ km, and $R_{\rm NS} = 35.4$ km for $t = 0.2$ s; and $R_{\rm ES} = 11.8$ km, $R_{\rm TS} = 12.7$ km, and $R_{\rm NS} = 12.1$ km for $t = 6$ s. We checked that using the averaged quantities or the energy-dependent ones does not influence our results in particular for the accretion and the cooling phases that are those relevant for neutrino decay in matter.

Figures 5 and 6 present the neutrino fluxes as a function of neutrino energy for the NS and the BH cases, respectively. The results correspond to ν_e, $\bar{\nu}_e$ and to the sum of non-electron flavors $(\nu_\mu, \nu_\tau, \bar{\nu}_\mu, \bar{\nu}_\tau)$ denoted as ν_x. As one can see from the figure, while the decay of $\bar{\nu}_e$ produces a depletion of the corresponding flux, the ν_e fluxes increase due to the $\bar{\nu}_e$ and $\bar{\nu}_x$ decay. Similarly, the sum of the ν_x fluxes shows both an increase and a decrease due to neutrino decay. Indeed, it presents an increase at low energies, and a decrease at high energies, due to the decay of the $\bar{\nu}_x$ into ν_e, $\bar{\nu}_e$, and ν_x.

In the following, we shall use the simulations from the Garching group first to extract from SN1987A neutrino events new bounds on neutrino-Majoron bounds from neutrino decay in matter. Then, we shall use Nakazato simulations and the same simulations from the Garching group to make prospects on the limits for neutrino-Majoron couplings from neutrino decay in matter if a future galactic core-collapse supernova leaves a newly born NS as remnant. It is to be noted that our analysis could be improved in the future by considering continuous variations in reasonable priors for the supernova neutrino emission parameters defining neutrino fluxes, as often done in the literature [21, 70]. However, our analysis also requires detailed information on the electron fraction and the matter density profiles as a

JCAP02(2026)069

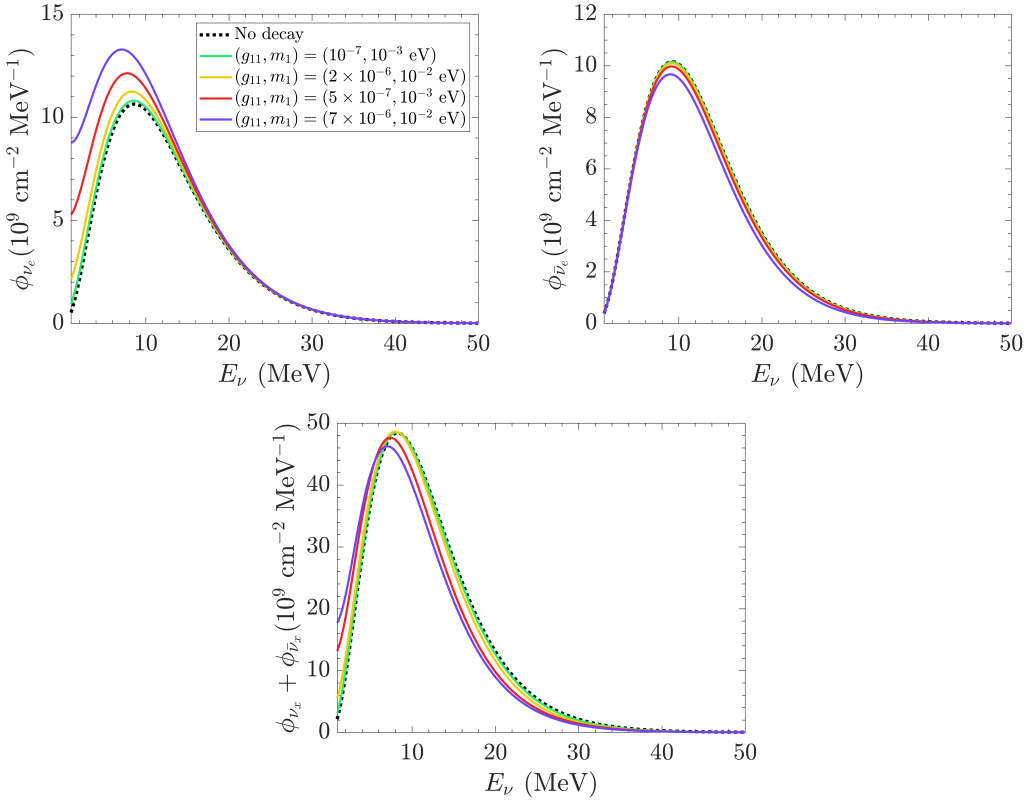

Figure 5. *NS case:* neutrino fluxes from a future core-collapse supernova, as a function of neutrino energy, and impact of neutrino non-radiative decay for the case where a NS is formed. The one-dimensional core-collapse supernova model used here is for a NS with 1.44 $M_\odot$ mass and the SFHx EOS (named 1.44SFHx) from the Garching simulations [46, 47]. The results shown are valid for normal neutrino mass ordering and include neutrino-Majoron interactions with different values of the lightest neutrino mass m_1 and of the g_{11} neutrino-Majoron coupling. The flux predictions in the absence of neutrino-Majoron interactions are also shown for comparison (black dotted line). The core-collapse supernova is located at 10 kpc.

function of time that are not currently available apart for a set of models. For this reason we employ the set of above-mentioned detailed supernova simulations, and proceed with a similar statistical analysis as the one employed in refs. [31, 32, 47]. It is to be noted that the use of a larger set of models, consistently providing the time-dependent neutrino emission and supernova properties (matter density and electron fraction), which are necessary to determine the impact of neutrino decay in matter, might weaken the neutrino-Majoron bounds derived in the present work.

As for the supernova location we will consider either 10 kpc or 0.2 kpc, having in mind Betelgeuse as an example. Concerning the DSNB, we shall use the same models as templates to perform predictions in the presence and absence of neutrino nonradiative two-body decay in matter.

JCAP02(2026)069

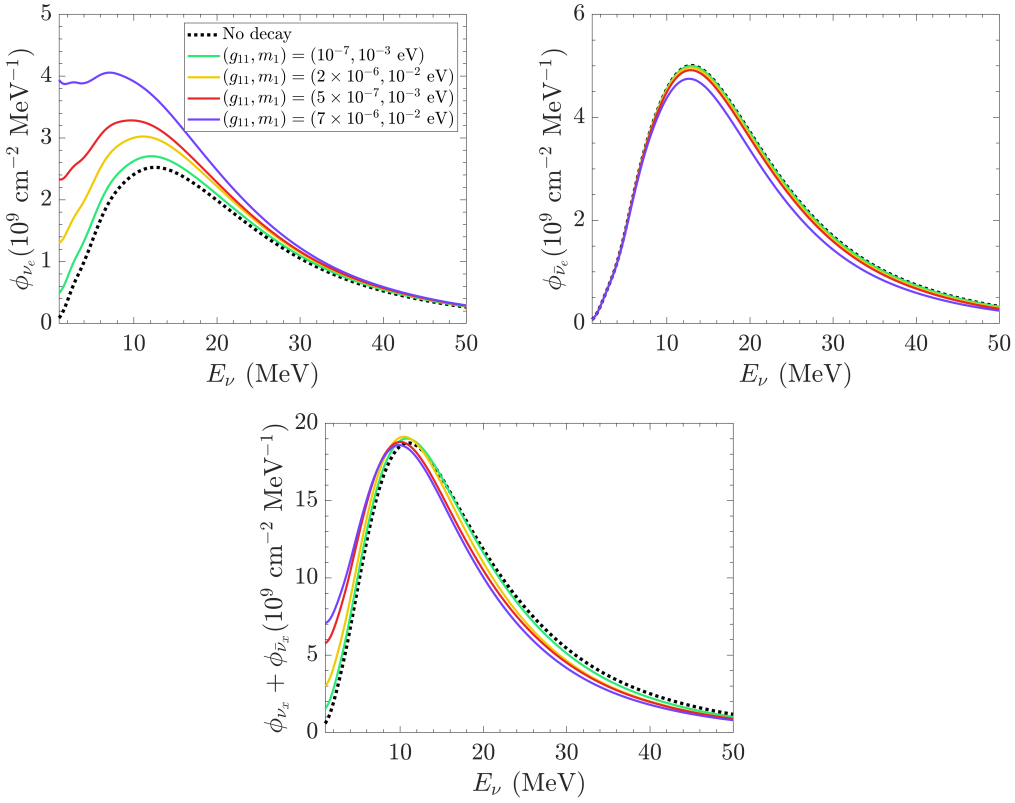

Figure 6. *BH case:* neutrino fluxes from a future core-collapse supernova, as a function of neutrino energy, and impact of neutrino non-radiative decay for the case where a BH is formed. The one-dimensional core-collapse supernova model used here is the 30 $M_\odot$ for the BH case from Nakazato simulations, with metallicity $Z = 0.004$ and the Togashi EOS [48, 49, 61]. The results are valid for normal neutrino mass ordering and include neutrino-Majoron interactions with different values of the lightest neutrino mass m_1 and of the g_{11} neutrino-Majoron couplings. The flux predictions in the absence of neutrino-Majoron interactions are also shown for comparison (black dotted line). The core-collapse supernova is located at 10 kpc.

4 New bounds on neutrino-Majoron couplings from SN1987A

The observation of SN1987A, located 50 kpc away, marked the first and, so far, only detection of neutrinos emitted from a core-collapse supernova. Three detectors, Kamiokande-II (2.14 kton), IMB (6.8 kton), and Baksan (0.28 kton), recorded 11, 8, and 5 $\bar{\nu}_e$ events, respectively [2–4]. The dominant process in these detectors was inverse beta decay (IBD). More information about these events can be found in ref. [21]. For the likelihood analysis, we follow [21, 71], and implement detailed information on the response of each of the detectors included in the analysis. A complete description of the statistical analysis and precise inputs can be found in appendix A.

Before presenting the results, we would like to emphasize that in the present work, we determine limits on neutrino-Majoron couplings considering that Majorons are free-streaming. Thus, our bounds are valid only in the free-streaming regime. It is to be noted, however, that in the very dense regions of the inner core, Majorons and neutrinos can be trapped so that

JCAP02(2026)069

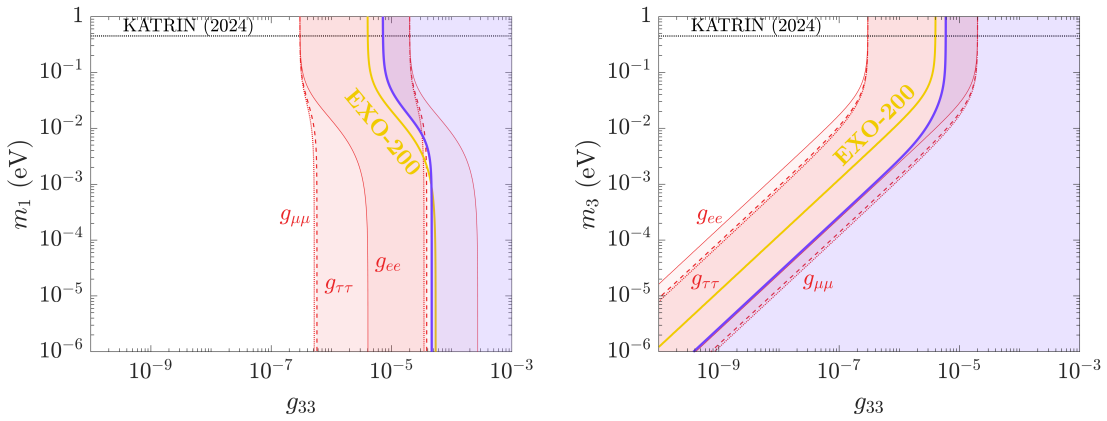

Figure 7. Constraints on the neutrino-Majoron coupling in the g_{33}–$m_{1,3}$ plane from our SN1987A analysis (blue) for normal at 68% CL.(left) and inverted ordering (right panel) at 90% CL. For comparison, we show the constraints obtained by the Majoron luminosity argument (red), which usually considers only one neutrino flavor at a time from ref. [33], along with the tightest limits from $0\nu\beta\beta$ decay (yellow solid line) [72]. The red-shaded areas are obtained by requiring the limit from ref. [33] on g_{ee} (red solid line), $g_{\mu\mu}$ (red dotted line), and $g_{\tau\tau}$ (red dashed line). Additionally, the current limit on the absolute neutrino mass obtained by the KATRIN experiment is also shown [73].

neutrino-Majoron and Majoron-Majoron scattering can be important, as well as Majoron decay to neutrinos. Moreover, neutrino scattering mediated by Majorons is possible.

A complete treatment would require self-consistent simulations solving neutrino transport in the stellar core, including Majorons which is beyond the scope of the present work. It is to be noted that bounds on neutrino-Majoron couplings, available in the literature, do not use such a theoretical framework, and are always given in the free-streaming regime. Refs. [39] and [40] are an exception, since the authors performed core-collapse supernova simulations with Majorons, but with the goal of assessing their impact on the stellar collapse, for the latter in the case of a massive Majoron. In this respect, it is to be noted that our bounds lie in a region where weak processes dominate over neutrino scattering mediated by Majorons for the case of inverted neutrino mass ordering, whereas for the normal mass ordering if $m_1 > 3 \times 10^{-3}\,\text{eV}$. Very small m_1 values might require a treatment beyond the free-streaming approximation we employ (see eq. (6b) of ref. [39]). So neutrino scattering mediated by Majorons should not impact the core-collapse supernova dynamics in the range of couplings of our bounds.

4.1 Limits on (g, m)

Neutrino-Majoron bounds in the mass basis. We will now present results using the simulation inputs from the 1.44SFHx supernova model, as a reference model for SN1987A. As discussed in ref. [47], this model is the one that better accounts for SN1987A observations. For the likelihood analysis, the numerical results are obtained using the simplex method. We employ the mass-squared differences $\Delta m^2_{21} = 7.53 \times 10^{-5}\,\text{eV}^2$ and $\Delta m^2_{32} = 2.437\ (-2.519) \times 10^{-3}\,\text{eV}^2$ for normal (inverted) neutrino mass orderings [9].

JCAP02(2026)069

Figure 7 shows our constraints in the neutrino mass basis, and in particular the ones on g_{33}, which were never shown before, as a function of the lightest neutrino mass, for normal and inverted ordering. The blue area represents the region excluded by our SN1987A likelihood analysis, considering the neutrino spectral distortions due to neutrino decay. The areas excluded by the Majoron luminosity argument ($3 \times 10^{-7} < |g_{\alpha\beta}| < 2 \times 10^{-5}$) [33] are shown in red for comparison. It is to be noted that the luminosity constraints are commonly obtained by assuming only one coupling at a time. For that reason, we show the bounds requiring the limit only on g_{ee} (red solid line), $g_{\mu\mu}$ (red dotted line), and $g_{\tau\tau}$ (red dashed line). Searches for Majoron-emitting neutrinoless double beta decay ($0\nu\beta\beta J$) have been performed for many years. Here, we show the tightest limit obtained from $0\nu\beta\beta$ decay translated into the g_{33}–m_1, or g_{33}–m_3 plane. This limit, currently coming from the EXO-200 [72], is represented by the yellow solid line.

Our results can be directly compared to those from [33, 34]. Our bounds for g_{11} improve on the ones from the spectrum analysis in [33] by more than an order of magnitude in normal ordering and by almost 2 orders of magnitude for $m_3 \gtrsim 10^{-2}\,\text{eV}$ in inverted ordering. Additionally, the limits we obtain for g_{22} are over an order of magnitude stronger than those reported in ref. [34]. Note that a comparison for g_{33} is not possible since this coupling was set to zero in ref. [34].

Neutrino-Majoron bounds in the flavor basis. The neutrino-Majoron coupling matrix in the flavor basis is related to the one in the mass basis through the relation

$$g_{\alpha\beta} = U_{\alpha i} g_{ij} U^{\dagger}_{j\beta}\,. \tag{4.1}$$

Our results on the neutrino-Majoron bounds, presented in the previous section, translated to the flavor basis, are shown in figure 8, both in normal and inverted neutrino mass ordering.

For the g_{ee} coupling, our limits can be compared to the ones established by $0\nu\beta\beta$ decay experiments. Table 2 summarizes the upper bounds on $|g_{ee}|$ obtained from our SN1987A analysis and those from such experiments. The ranges shown for our results reflect the dependence on m_1 for normal ordering and m_3 for inverted ordering. For the $0\nu\beta\beta$ results, the indicated ranges account for the uncertainties in the nuclear matrix elements. From table 2, one can see that our limits are competitive with those from $0\nu\beta\beta$ decay experiments, and are surpassed by EXO-200 results only [72]. It is important to note that the results presented in table 2 are the tightest limits obtained at each experiment, corresponding to $0\nu\beta\beta J$ models with one Majoron emission. Other models considered in their analyses yield significantly looser bounds (see ref. [72]).

It is to be noted that $0\nu\beta\beta$ decay experiments can only probe the g_{ee} element of the flavor coupling matrix. For the other couplings, we can only compare them to the limits from the luminosity argument or meson and lepton decays. On the other hand, the limits obtained from meson and lepton decays constrain certain combinations of the coupling elements rather than individual ones. A detailed comparison to these limits was presented in our previous work [36] where we showed that our bounds on the $\sum_\beta g^2_{\alpha\beta}$ ($\alpha, \beta = e, \mu, \tau$) improve by $4 - 7$ orders of magnitude the bounds derived from meson and lepton decay data [79, 80].

JCAP02(2026)069

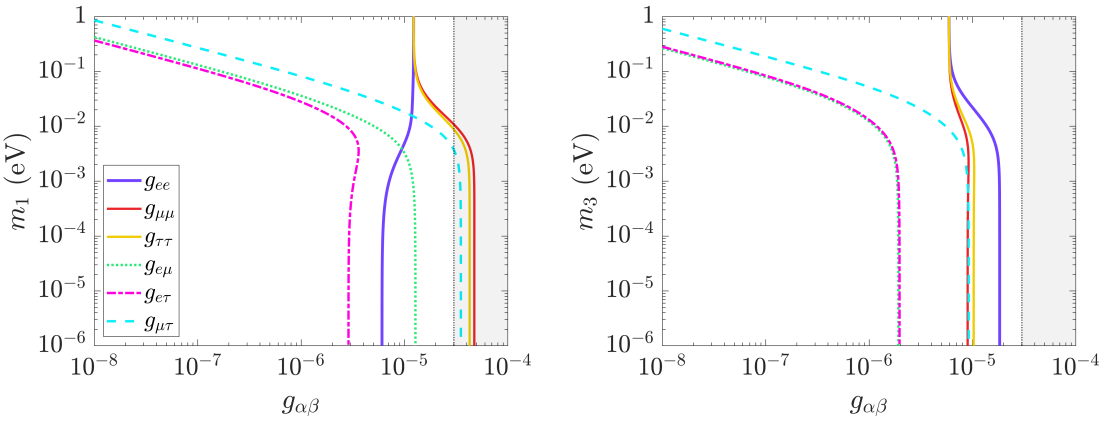

Figure 8. Constraints on the neutrino-Majoron couplings in the flavor basis at 90% CL, as a function of the lightest neutrino mass, namely m_1 for normal (left panel) and m_3 for inverted (right panel) neutrino mass ordering. The results shown are obtained from our likelihood analysis of the spectral distortion of SN1987A neutrino events. The excluded areas are to the right of the lines. The bands (light grey) indicate the region where the free-streaming approximation migh be replaced by a more extended treatment including e.g. neutrino scattering mediated by Majorons (see text).

Analysis	Reference		$\lvert g_{ee}\rvert$ bounds
SN1987A (NO)	**This work**		$\mathbf{(0.6-1.2)\times 10^{-5}}$
SN1987A (IO)	**This work**		$\mathbf{(0.6-1.8)\times 10^{-5}}$
$0\nu\beta\beta J$ (^{136}Xe)	EXO-200	[72]	$(0.4-0.9)\times 10^{-5}$
$0\nu\beta\beta J$ (^{136}Xe)	KamLand-Zen	[74]	$(0.8-1.6)\times 10^{-5}$
$0\nu\beta\beta J$ (^{100}Mo)	NEMO-3	[75]	$(1.6-3.0)\times 10^{-5}$
$0\nu\beta\beta J$ (^{82}Se)	CUPID-0	[76]	$(1.8-4.4)\times 10^{-5}$
$0\nu\beta\beta J$ (^{76}Ge)	GERDA	[77]	$(1.8-4.4)\times 10^{-5}$
$0\nu\beta\beta J$ (^{100}Mo)	CUPID-Mo	[78]	$(4.0-6.9)\times 10^{-5}$

Table 2. Upper bounds on $|g_{ee}|$ from different analyses. The limits derived from SN1987A were obtained using the 1.44SFHx supernova model of ref. [47]. The corresponding ranges reflect the dependence on the lightest neutrino mass. In contrast, the ranges in the $0\nu\beta\beta J$ results account for the uncertainties in the nuclear matrix elements.

JCAP02(2026)069

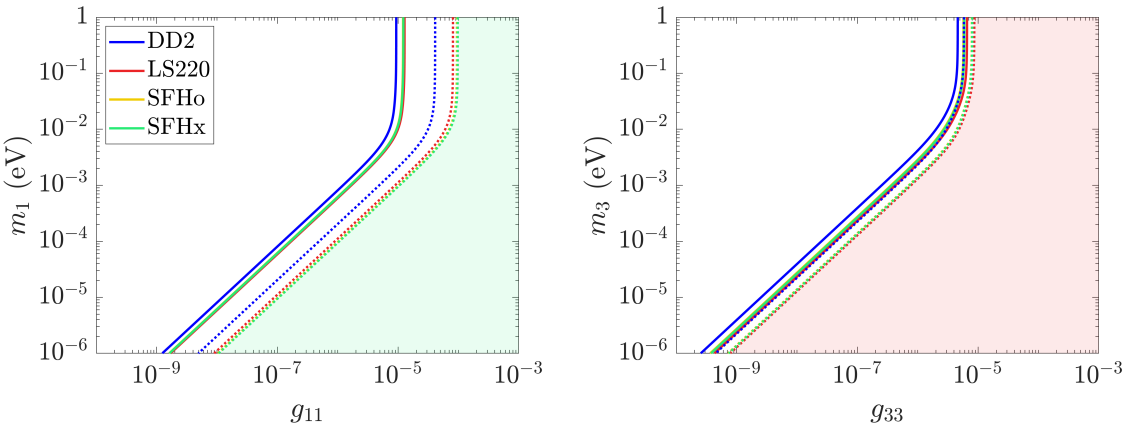

Figure 9. Comparison of our 90% CL results for the eight models considered: 1.44$M_\odot$ (solid lines) and 1.62$M_\odot$ (dotted lines), each with four different equations of states (see legend). The left panel displays results in the g_{11}–m_1 plane for normal ordering, while the right panel shows results in the g_{33}–m_3 plane in the inverted ordering case. Shaded areas represent the most conservative excluded regions. Results from equations of state SFHo and SFHx are nearly identical, the corresponding lines being almost indistinguishable.

4.2 Comparison of results with different models

We investigated the dependence of our bounds on the SN1987A model used. To this aim, figure 9 compares the bounds derived using different core-collapse supernova models. The shaded areas indicate the most conservative excluded regions. The figure presents the results in the g_{11}–m_1 plane for normal mass ordering. In this case, the 90% CL limits span approximately an order of magnitude. All the 1.44 $M_\odot$ models (solid lines) produce similar results, while the 1.62 $M_\odot$ models (dotted lines) yield looser limits. Additionally, one should note that the equations of state SFHo and SFHx give almost indistinguishable results. Figure 9 also shows the bounds in the g_{33}–m_3 plane obtained for the inverted mass ordering. Here, the bounds spread over approximately half an order of magnitude. This suggests that our limits in the inverted ordering case are practically model-independent (for the ensemble of models considered in the present work).

5 Prospects on the neutrino-Majoron couplings from a future supernova

Thanks to their larger fiducial volumes, the next generation of neutrino detectors will be able to observe the neutrino flux from a future galactic core-collapse supernova with significantly higher statistics compared to SN1987A. Additionally, as pointed out by ref. [81], dark matter detectors will also be sensitive to the total supernova neutrino fluxes, offering complementary observations. We consider here some of the supernova neutrino observatories included in the upgraded version of the Supernova Neutrino Early Warning System (SNEWS 2.0). These are the HK experiment, expected to start running in 2028 [82], the JUNO experiment that will start in 2025–2026 [83], the DUNE experiment that will be operating in a staged approach between 2029 and 2032 [84], and finally the DARWIN experiment [85].

JCAP02(2026)069

Experiment	Channel	$N_{\rm t}$	E_{th} (MeV)	ref.
HK	IBD	1.25×10^{34}	5	[86, 87]
	ES	6.25×10^{34}	5	[88]
JUNO	IBD	1.21×10^{33}	5	[86, 87]
	pES	1.21×10^{33}	0.3	[89]
DUNE	ν_e-^{40}Ar	6.02×10^{32}	5	[90]
DARWIN	CEνNS	1.83×10^{29}	10^{-3}	[81]

Table 3. Parameters characterizing the experiments and detection channels. The quantities $N_{\rm t}$ and E_{th} refer to the number of targets and the energy threshold, respectively, while the last column gives the reference for the cross section associated with the main detection channel of the corresponding experiment. For all experiments, an idealized efficiency of 100% was applied.

After presenting the details of the response functions and the inputs used for each of these supernova neutrino observatories, we will present here our predictions for the expected number of events associated with a galactic core-collapse supernova neutrino signal, both in the presence and in the absence of neutrino decay. Then we will show the outcome of our 2-dimensional likelihood analyses of the spectral distortions induced by neutrino decay in an exploding core-collapse supernova, and the bounds on the neutrino-Majoron couplings in case such a rare event takes place.

5.1 Experiments

The expected signal rate at each of the future detectors considered, as a function of the reconstructed energy E_r, is calculated through the following expression

$$\frac{dS}{dE_r} = \eta \int_0^\infty G(E_t - E_r, \delta(E_r)) \frac{dS_t}{dE_t} dE_t \,, \tag{5.1}$$

where dS_t/dE_t represents the true signal distribution as a function of the true energy E_t, and η denotes the efficiency, assumed here to be energy-independent. For all experiments, we considered the idealized case of 100% efficiency, i.e., $\eta = 1$. The smearing function G is considered Gaussian with uncertainty function $\delta(E_r)$, specific to each detector.

We now present the experiments and the main detection channels of each detector under consideration. Table 3 shows the corresponding number of targets, energy thresholds, and the references for the associated cross sections used in our computations.

5.1.1 Hyper-Kamiokande

HK [82], currently under construction in Japan, is set to be the successor of SK. This water Cherenkov detector will have a fiducial volume of 187 kton, more than eight times that of SK. HK is expected to start taking data in 2028.

The main detection channel at HK will be IBD, making this detector predominantly sensitive to the supernova $\bar{\nu}_e$ flux. The true signal for this detection channel was calculated

JCAP02(2026)069

with eq. (5.1). For the reconstructed signal, we applied the uncertainty function given by [29]

$$\delta(E_r) = 0.1\sqrt{E_r[\mathrm{MeV}]}\,. \tag{5.2}$$

Additionally, HK will be capable of detecting supernova neutrinos via elastic scattering on electrons (ES):

$$\overset{(-)}{\nu}_\alpha + e^- \to \overset{(-)}{\nu}_\alpha + e^-, \text{ with } \alpha = e, \mu, \tau\,. \tag{5.3}$$

Although its cross-section is several orders of magnitude smaller than that of IBD, this detection channel is still valuable as it probes all neutrino flavors. The true signal for ES can be expressed as

$$\frac{dS_t}{dE_t} = N_t \int_{E_\nu^{\min}}^{\infty} \sum_\alpha \left[\sigma_{\mathrm{ES}-\nu_\alpha}(E_\nu, E_t)\phi_{\nu_\alpha}(E_\nu) + \sigma_{\mathrm{ES}-\bar{\nu}_\alpha}(E_\nu, E_t)\phi_{\bar{\nu}_\alpha}(E_\nu)\right] dE_\nu\,, \tag{5.4}$$

where E_t here represents the true kinetic recoil energy of the electron, and $E_\nu^{\min} \simeq E_t + m_e/2$ is the minimum energy necessary to induce a recoil E_t. The cross-section $\sigma_{\mathrm{ES}-\nu_\alpha}$ depends on the neutrino or antineutrino flavor. Finally, to compute the reconstructed signal for this channel, we used the following uncertainty function [29, 91]:

$$\frac{\delta(E_r)}{E_r} = 0.0349 + \frac{0.376}{\sqrt{E_r[\mathrm{MeV}]}} - \frac{0.123}{E_r[\mathrm{MeV}]}\,. \tag{5.5}$$

Other detection channels at HK include charged-current interactions of ν_e and $\bar{\nu}_e$ on oxygen nuclei that we will neglect since these channels are subdominant [92].

5.1.2 JUNO

The Jiangmen Underground Neutrino Observatory (JUNO) [83] is a liquid-scintillator neutrino experiment under construction in China. This detector will have a fiducial volume of 17 kton. As HK, the main detection channel of JUNO is IBD. The number of proton targets is $N_t = 1.21 \times 10^{33}$ for its fiducial volume. We took the energy resolution

$$\delta(E_r) = 0.03\sqrt{E_r[\mathrm{MeV}]}\,. \tag{5.6}$$

In addition, JUNO is sensitive to all neutrino flavors through elastic scattering of neutrinos on protons (pES):

$$\overset{(-)}{\nu}_\alpha + p \to \overset{(-)}{\nu}_\alpha + p, \text{ with } \alpha = e, \mu, \tau\,. \tag{5.7}$$

The cross-section of this interaction is around 3 times smaller than that of IBD. However, this lower cross-section is compensated for by the contribution of all flavors. The signal distribution as a function of the proton recoil energy E_t' is

$$\frac{dS_t}{dE_t'} = N_t \int_{E_\nu^{\min}}^{\infty} \left[\sigma_{\mathrm{pES}-\nu}(E_\nu, E_t') \sum_\alpha \phi_{\nu_\alpha}(E_\nu) + \sigma_{\mathrm{pES}-\bar{\nu}}(E_\nu, E_t') \sum_\alpha \phi_{\bar{\nu}_\alpha}(E_\nu)\right] dE_\nu\,, \tag{5.8}$$

JCAP02(2026)069

where we distinguish the pES cross-section for neutrinos $\sigma_{\mathrm{pES}-\nu}$ and antineutrinos $\sigma_{\mathrm{pES}-\bar{\nu}}$. The minimum neutrino energy needed to produce a recoil energy E'_t is

$$E_\nu^{\min} = \frac{E'_t + \sqrt{E'_t(E'_t + 2m_p)}}{2}\,. \tag{5.9}$$

One should take into account that the visible energy E_t in the detector is strongly quenched with respect to E'_t [89, 93, 94]. To convert from the true proton energy to the visible one, we used the quenching factor from [83], obtained using the results of [94]. The observed signal was obtained using the same uncertainty function as for the IBD channel.

5.1.3 DUNE

The upcoming Deep Underground Neutrino Experiment (DUNE) [84], in the United States, will also be able to detect supernova neutrinos. DUNE will consist of four 10-kton liquid argon time projection chambers, resulting in a total fiducial volume of 40 kton. This detector will be built in a staged approach starting from early 2029 up to 2032.

The main detection channel at DUNE will be CC interactions on liquid argon, which will allow probing the ν_e component of the supernova flux

$$\nu_e + {}^{40}\mathrm{Ar} \to e^- + {}^{40}\mathrm{K}^*\,. \tag{5.10}$$

The signal as a function of the true neutrino energy is

$$\frac{dS_t}{dE_\nu} = N_t \sigma_{\nu-\mathrm{Ar}}(E_\nu)\phi_{\nu_e}(E_\nu)\,. \tag{5.11}$$

We used the number of targets $N_t = 6.02 \times 10^{32}$. The cross-section $\sigma_{\nu-\mathrm{Ar}}$ was taken from `SNOwGLoBES` [90]. To obtain the reconstructed signal, we used the following uncertainty function [95]

$$\delta(E_r) = 0.2E_r. \tag{5.12}$$

5.1.4 DARWIN

DARk matter WImp search with liquid xenoN (DARWIN) [85] will be an experiment whose main purpose will be the direct detection of dark matter. In addition, it will also serve as a neutrino detector. DARWIN will consist of 40 tons of Xenon. This detector will be sensitive to neutrinos and antineutrinos of all flavors through Coherent Elastic Neutrino-Nucleus Scattering (CEνNS) measured for the first time in 2017 by the COHERENT Collaboration [96], more than 40 years after its predictions by Freedman [97].

The true signal as a function of the true nuclear recoil energy E_t is

$$\frac{dS_t}{dE_t} = N_t \int_{E_\nu^{\min}}^{\infty} \sigma_{\mathrm{CE}\nu\mathrm{NS}}(E_\nu, E_t) \sum_\alpha \left[\phi_{\nu_\alpha}(E_\nu) + \phi_{\bar{\nu}_\alpha}(E_\nu)\right] dE_\nu\,. \tag{5.13}$$

The minimum neutrino energy necessary to produce a recoil energy E_t is $E_\nu^{\min} \simeq \sqrt{m_N E_t/2}$, where m_N is the mass of the nucleus. For the reconstructed signal, we assumed an uncertainty function given by [29, 98]

$$\frac{\delta(E_r)}{E_r} = 0.077 + \frac{0.232}{\sqrt{E_r[\mathrm{keV}]}} - \frac{0.069}{E_r[\mathrm{keV}]}\,. \tag{5.14}$$

JCAP02(2026)069

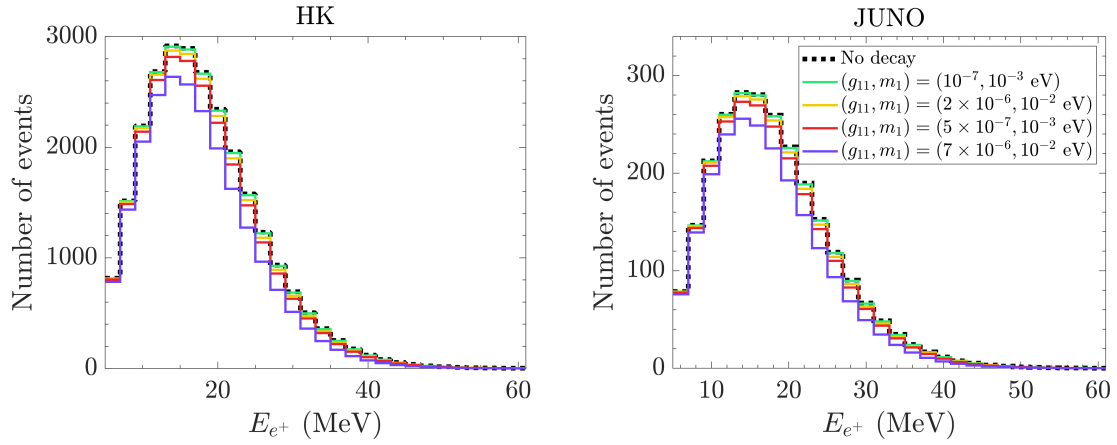

(a) 1.44SFHx (NS).

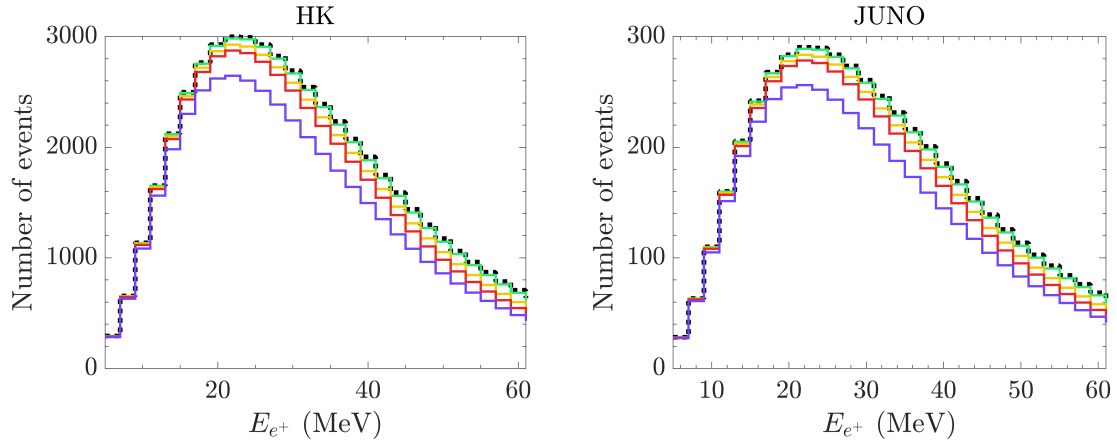

(b) 30T (BH).

Figure 10. Expected IBD events from a future core-collapse supernova at 10 kpc, assuming normal ordering and including neutrino-Majoron interactions for different values of g_{11} and m_1 compatible with current constraints. Predictions are given for HK and JUNO for the NS case using the 1.44SFHx model (top panels) and for the BH case using the 30T model (bottom panels). For comparison, the black dotted line shows the prediction in the absence of neutrino-Majoron interactions.

5.2 Predictions on the neutrino number of events

We present here our predictions for the number of events in the JUNO experiment, the near-future HK, as well as the more distant-future DUNE and DARWIN experiments. The computations were performed by considering a galactic core-collapse supernova at a nominal distance of 10 kpc, 8 kpc (corresponding to the galactic center), and 0.2 kpc (approximate distance to the supernova candidate Betelgeuse). While the distance simply acts as a scaling factor for the number of events, it is still interesting to examine its influence on the projected bounds on the neutrino-Majoron couplings.

Figure 10 presents the expected IBD events as a function of positron energy in HK and JUNO, assuming normal mass ordering. The results correspond to the 1.44SFHx model from the Garching simulations for the NS case and the 30T model from Nakazato's simulations for the BH case. The predictions are shown for the no-decay scenario and for neutrino decay

JCAP02(2026)069

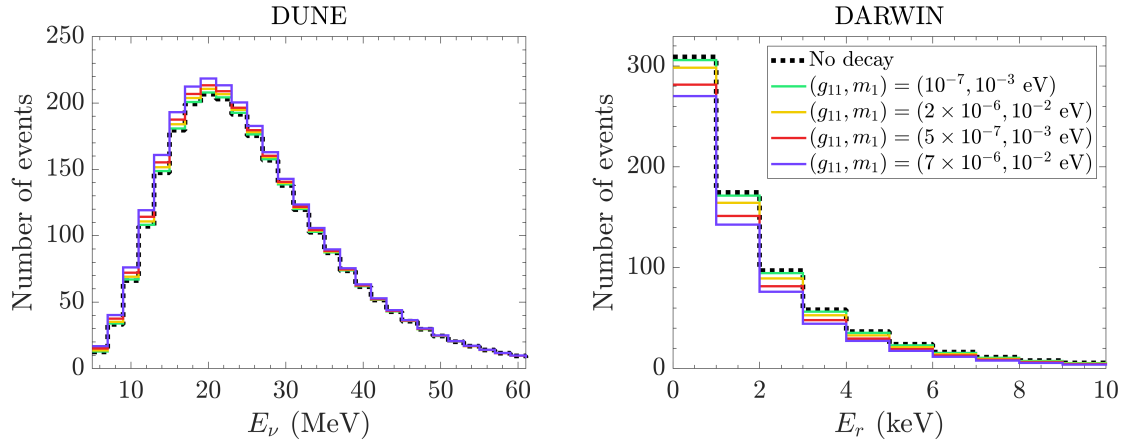

(a) 1.44SFHx (NS).

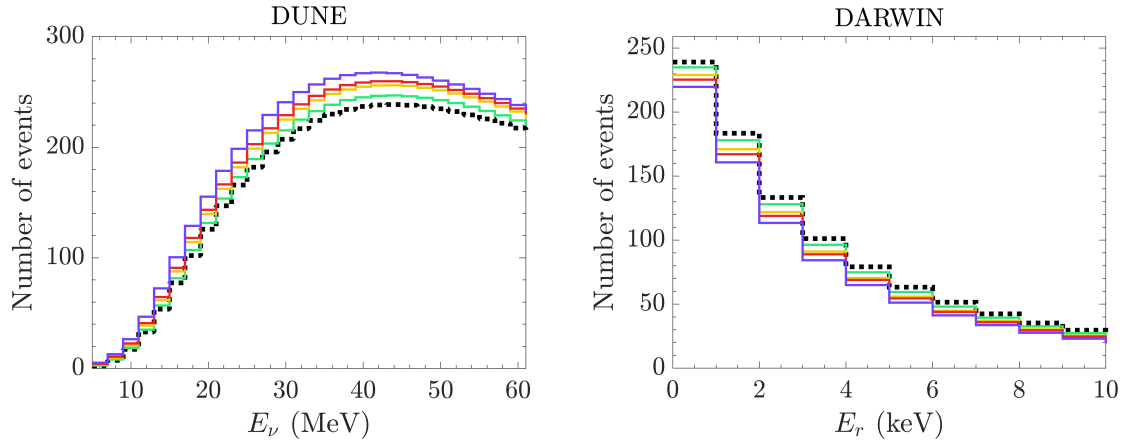

(b) 30T (BH).

Figure 11. Expected events from a future core-collapse supernova located at 10 kpc, assuming normal ordering and including neutrino-Majoron interactions for different values of g_{11} and m_1 compatible with current constraints. Predictions correspond to ν-Ar scattering in DUNE and to coherent neutrino-nucleus scattering in DARWIN for the NS case using the 1.44SFHx model (top panels) and for the BH case using the 30T model (bottom panels). For comparison, the black dotted line shows the prediction in the absence of neutrino-Majoron interactions.

with several values of the g_{11} coupling and the lightest neutrino mass m_1. Similarly, figure 11 shows the expected ν–^{40}Ar events at DUNE as a function of neutrino energy, along with the CEνNS events at DARWIN. These results are also shown for normal ordering and for the NS and BH cases using the 1.44SFHx and 30T models, respectively. Note that the effect of decay in matter is modest in the ES signal at HK and in the pES signal at JUNO (see appendix B). For the NS case, we find that decay effects are negligible in inverted ordering across all detectors and detection channels. In contrast, for the BH case, the dominant channels exhibit visible effects due to decay in inverted ordering (see appendix B). In this case, the IBD rates are overall smaller than in normal ordering, although the decay-induced suppression is more pronounced in inverted ordering for the BH case. Conversely, for DUNE and DARWIN, the impact of decay is reduced in inverted ordering compared to normal ordering.

JCAP02(2026)069

	No decay	$g_{11} = 10^{-7}$ $m_1 = 10^{-3}$ eV	$g_{11} = 2 \times 10^{-6}$ $m_1 = 10^{-2}$ eV	$g_{11} = 5 \times 10^{-7}$ $m_1 = 10^{-3}$ eV	$g_{11} = 7 \times 10^{-6}$ $m_1 = 10^{-2}$ eV
HK-IBD	26085	25957	25444	24794	22441
	(58362)	(57298)	(53858)	(51777)	(47047)
HK-ES	1190	1185	1174	1154	1143
	(1516)	(1506)	(1498)	(1497)	(1494)
JUNO-IBD	2525	2513	2463	2400	2173
	(5650)	(5547)	(5214)	(5012)	(4554)
JUNO-pES	459	426	377	348	304
	(3997)	(3637)	(3363)	(3291)	(3060)
DUNE	2452	2467	2498	2530	2588
	(10489)	(10821)	(11212)	(11351)	(11580)
DARWIN	406	394	369	337	313
	(870)	(816)	(767)	(749)	(708)

Table 4. Expected total number of events from a future supernova located at 10 kpc, including neutrino-Majoron interactions producing neutrino nonradiative two-body decay in matter. The results are for the case of normal mass ordering. The first column shows the detection channels of the four experiments considered. The second column shows the results in the absence of decay, while the other columns give the expected values for different values of the neutrino-Majoron couplings g_{11} and the lightest neutrino mass m_1. The values correspond to the NS case with the 1.44SFHx model and to the BH case with the 30T model (in parentheses).

Table 4 shows the total number of events in normal ordering, assuming fixed values of g_{11} and m_1. (The results in inverted mass ordering can be found in appendix B.) The results are given for the NS case using the 1.44SFHx model, and for the BH case with the 30T model. To compare the impact of decay in different scenarios, table 5 presents the number of events for the no-decay case and for the case with the largest decay effects, along with the corresponding ratio. These values are provided for both normal and inverted ordering, and for the NS and BH cases using the 1.44SFHx and 30T models, respectively. Note that the largest decay effects are obtained for $g_{11} = 7 \times 10^{-6}$ and $m_1 = 10^{-2}$ eV for normal ordering and $g_{33} = 10^{-6}$ and $m_3 = 10^{-2}$ eV for inverted ordering.

5.3 Prospects on the neutrino-Majoron couplings

It is interesting to determine the sensitivity to the neutrino-Majoron couplings that will be obtained from the observation of the next galactic core-collapse supernova. To that aim, we perform a likelihood analysis of simulated data (for details on the analysis, see appendix A). Considering the IBD events in HK, the ν–^{40}Ar events in DUNE, and the CEνNS events in DARWIN, we simulate the events at these detectors assuming a *true* model without neutrino-Majoron interactions, and extract constraints by comparing it to a set of *test* models including such interactions and profiling over this set of test models.

We assume that the large signal from the next galactic event will allow identification of the remnant (NS or BH), and accordingly, restrict the profiling to models with the same outcome as the true model. For the NS case, we consider two true models: 1.36DD2 and 1.62SFHx, chosen from the Garching group simulations for their distinct standard fluxes and

JCAP02(2026)069

	NS			BH		
	No decay	Largest effect	Ratio	No decay	Largest effect	Ratio
HK-IBD	26085	22441	0.86	58362	47047	0.81
	(27884)	(26304)	(0.94)	(42560)	(31888)	(0.75)
HK-ES	1190	1143	0.96	1516	1494	0.99
	(1169)	(1164)	(1.00)	(1631)	(1617)	(0.99)
JUNO-IBD	2558	2204	0.86	5659	4563	0.81
	(2736)	(2583)	(0.94)	(4126)	(3093)	(0.75)
JUNO-pES	459	304	0.66	3997	3060	0.77
	(459)	(423)	(0.92)	(3997)	(3597)	(0.90)
DUNE	2452	2588	1.06	10489	11580	1.10
	(2136)	(2170)	(1.02)	(10982)	(11631)	(1.06)
DARWIN	406	313	0.77	870	708	0.81
	(406)	(393)	(0.97)	(870)	(810)	(0.93)

Table 5. Expected total number of events from a future supernova located at 10 kpc, including neutrino-Majoron interactions, for the case of no decay (second column) and for the largest effect produced by neutrino-Majoron interaction (third column). The fourth column gives the ratio between the largest effect and the no-decay case. Results are given for normal ordering and inverted ordering (in parentheses). The largest decay effects are obtained for $g_{11} = 7 \times 10^{-6}$ and $m_1 = 10^{-2}$ eV for normal ordering and $g_{33} = 10^{-6}$ and $m_3 = 10^{-2}$ eV for inverted ordering. Results were obtained for the NS case using the 1.44SFHx model and for the BH case using the 30T model (shown in columns fifth to seven).

decay effects. These "extreme" cases help assess the model dependence of the results. The profiling includes these two and an intermediate model, 1.44SFHx. For the BH case, the true models considered are 30T and 30S, selected among the three models from Nakazato's simulations. The profiling is performed over all three: 30L, 30T, 30S.

For each possible outcome, NS or BH, we found the projected bounds to be nearly equal for the two true models considered. Therefore, in the following, unless otherwise stated, we only show the results for the 1.62SFHx model in the NS case and the 30T model in the BH case. Figure 12 presents a comparison of the projected bounds with current limits on the neutrino-Majoron coupling. Both the results for the NS case in normal and inverted mass ordering and the BH case ones are given. The figure also shows a comparison of our bounds from our SN1987A reference analysis and the current most optimistic limits from EXO-200 [72]. Moreover the limits from the luminosity argument from [33] applied to the couplings g_{ee}, $g_{\mu\mu}$, and $g_{\tau\tau}$ are shown. One can see that the projected bounds from a future supernova improve significantly upon those from SN1987A, especially if a BH is formed. Such improvement is essentially coming from the increased statistics.

To assess how our projected bounds would improve upon current limits from laboratory experiments, we translate them into the g_{ee}–$m_{1,3}$ plane. Figure 13 shows the results for the NS and the BH cases, considering both mass orderings, in comparison with the ones from the luminosity argument ref. [33] and from EXO-200 [72], NEMO-3 [75], and CUPID-0 [76] experiments. Also shown is how the bounds vary due to the uncertainty of the neutrinoless double-beta decay nuclear matrix elements.

JCAP02(2026)069

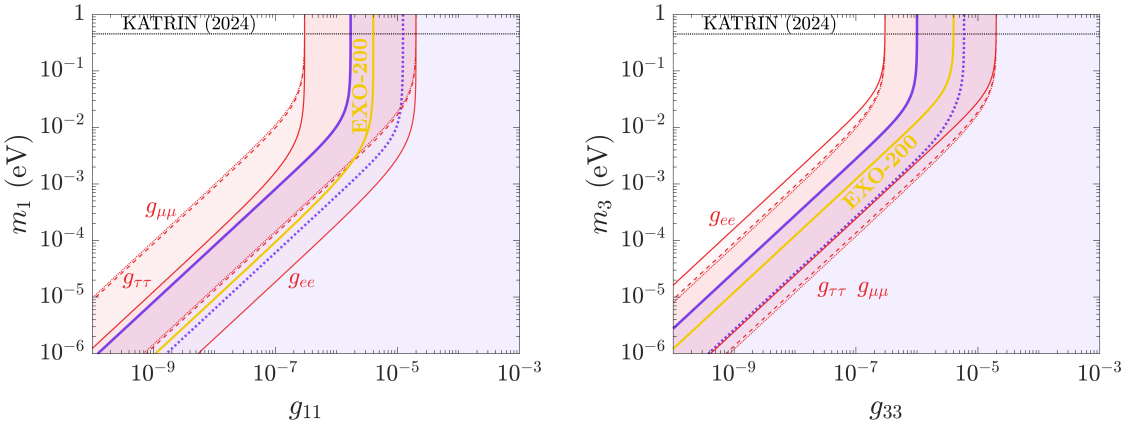

(a) True model: 1.62SFHx (NS).

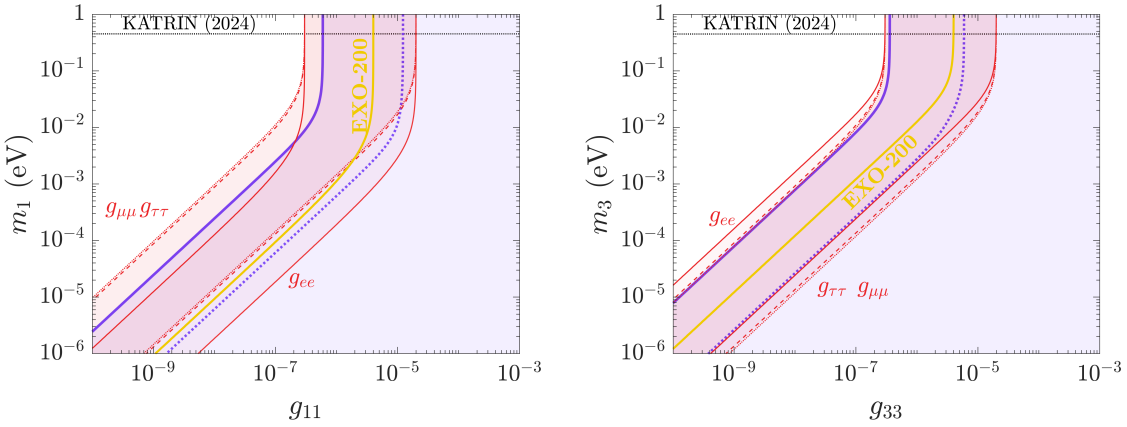

(b) True model: 30T (BH).

Figure 12. Projected bounds on the neutrino-Majoron coupling in the g_{ii}–m_i plane, with $i = 1$ for normal ordering (left panels) and $i = 3$ for inverted ordering (right panels), for a NS-forming collapse (top panels) and a BH-forming collapse (bottom panels) at 10 kpc. Solid blue lines show the 90% CL limits from this analysis, while dotted blue lines indicate the corresponding constraints from our SN1987A reference study. For comparison, we include bounds from the Majoron luminosity argument from ref. [33] (red shaded regions and lines), obtained assuming one active flavor-coupling at a time, and the most stringent current limits from neutrinoless double-beta decay experiments (solid yellow line), obtained by EXO-200 with the most optimistic nuclear matrix element [72]. The upper limit on the absolute neutrino mass from KATRIN is also shown [73]. Note that the bounds are obtained here by profiling on the other models for the same case (see text).

JCAP02(2026)069

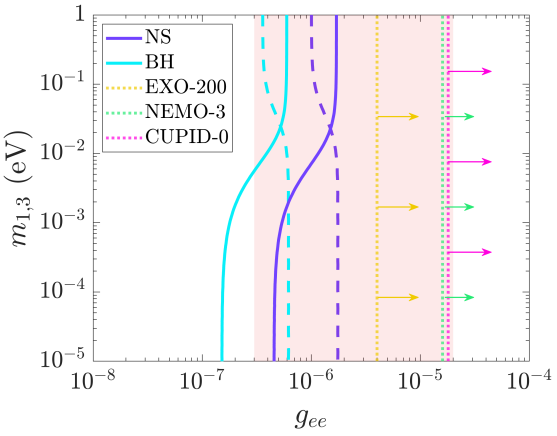

Figure 13. Projected bounds on the neutrino-Majoron coupling g_{ee} from neutrino decay in matter, as a function of the lightest stable neutrino mass eigenstate m_1 for normal (blue solid lines) and m_3 for inverted (blue dashed lines) mass orderings. The results shown correspond to the NS case (NSFC) using the 1.62SFHx model and the BH case (BHFC) with the 30T model. For comparison, the most stringent limits for massless Majorons from neutrinoless double-beta decay experiments are also given, for the EXO-200 [72], NEMO-3 [75], and CUPID-0 [76] experiments. The uncertainties from the nuclear matrix elements are shown by the arrows. The red band corresponds to the constraint from the supernova cooling argument [33].

In order to highlight the role of the different experiments in determining the bounds, we show the projected bounds from individual cases in figure 14, along with the result of the combined analysis. The results are in normal ordering for the NS case, assuming a distance of 10 kpc, for HK, DUNE, DARWIN, along with those from the combined analysis. This comparison highlights the dominant role of HK, whose strong sensitivity largely drives the results of the combined analysis.

Finally, it is interesting to look at the dependence of the limits on neutrino-Majoron couplings from neutrino decay in matter on the possible location of the supernova. This is shown in figure 14, where results for the NS case and a distance of 10 kpc, 8 kpc, and 0.2 kpc are given. Interestingly, a close supernova located at 0.2 kpc would result in bounds nearly an order of magnitude larger than those from an event at 10 kpc.

6 Neutrino decay in matter and impact on the Diffuse Supernova Neutrino Background

After investigating the prospects of setting improved limits on neutrinos coupling to Majorons from the next supernova, we turn to the case of the DSNB, whose discovery might lie in the foreseeable future. Here we present the results of the first investigation of how neutrino non-radiative two-body decay in matter can influence the DSNB. The DSNB flux, produced by past core-collapse supernova explosions, needs important information from cosmology, astrophysics, and neutrino physics. As such, its observation will bring unique information with respect to individual core-collapse supernovae. We will show how this process impacts the DSNB fluxes and event rates in the JUNO, upcoming Hyper-K, and near-future DUNE

JCAP02(2026)069

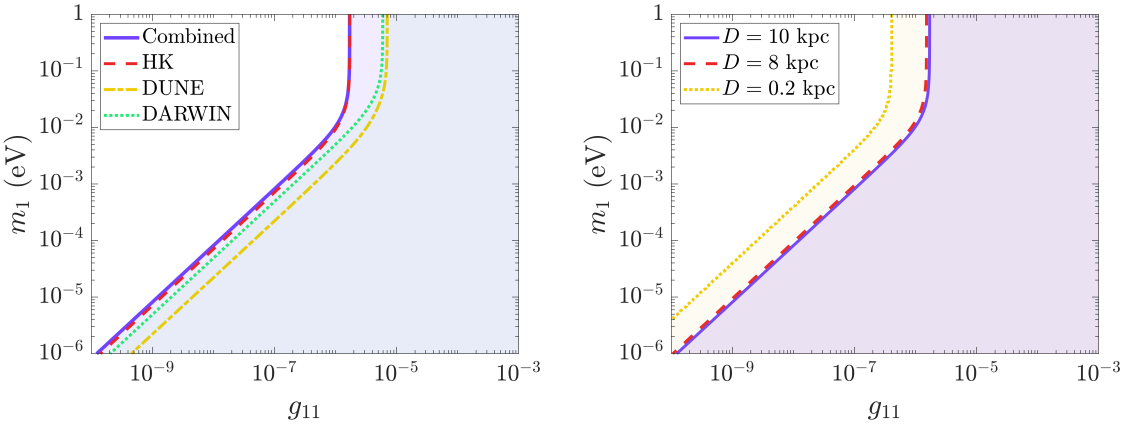

Figure 14. Limits on the neutrino-Majoron coupling g_{11} (90 % C.L.) as a function of the lightest mass eigenstate m_1 in the case of neutrino normal mass ordering. The results shown are obtained by considering 1.62SFHx as the true model and profiling over the others. Left figure: bounds from signals at individual detectors, and from their combination. The results are for a supernova at 10 kpc. Right figure: bounds vary depending on the supernova core-collapse supernova distance, taken from the nominal value of 10 kpc, to 8 kpc (galactic center), to about 0.2 kpc (distance of Betelgeuse) as examples.

and DARWIN experiments. But let us first see the theoretical framework of our study and the scenarios we considered. Note that here we employ the parametrization commonly used. Recently, a new parametrization based on the compactness has been suggested [99].

6.1 The DSNB flux

The DSNB flux reads

$$F_{\nu_i}(E_\nu) = c \int_0^\infty \mathrm{d}z \left[\int_\Omega \mathrm{d}M R_{\mathrm{SN}}(z, M) \phi_{\nu_i,\mathrm{NS}}(E'_\nu, M) + \int_\Sigma \mathrm{d}M R_{\mathrm{SN}}(z, M) \phi_{\nu_i,\mathrm{BH}}(E'_\nu, M) \right] (1+z) \left| \frac{\mathrm{d}t_\mathrm{c}}{\mathrm{d}z} \right| . \tag{6.1}$$

Here c is the speed of light, z the cosmological redshift, M is the progenitor mass, $E'_\nu = (1+z)E_\nu$ is the redshifted neutrino energy, and $|\mathrm{d}t_\mathrm{c}/\mathrm{d}z|$ the cosmic time. The two terms in the integral (6.1) depend on the evolving core-collapse supernova rate $R_{\mathrm{SN}}(z, M)$ and the neutrino yields $\phi_{\nu_i,\mathrm{NS}}(E'_\nu, M)$ and $\phi_{\nu_i,\mathrm{BH}}(E'_\nu, M)$ correspond to the contributions from core-collapse supernovae leaving either a neutron-star (NS) or a black-hole (BH). The terms Ω and Σ indicate the relative progenitor mass domains. In our computations, we considered $z \in [0, 5]$ and progenitor masses in the range $M \in [8, 125] M_\odot$.

For the evolving core-collapse supernova rate, we used

$$R_{\mathrm{SN}}(z, M) = \frac{\dot{\rho}_*(z)\phi(M)}{\int_{0.5M_\odot}^{125M_\odot} \phi(M) M \, dM} . \tag{6.2}$$

with the initial mass function (IMF) $\phi(M)$ such that $\phi(M)\mathrm{d}M$ is the number of stars in the mass interval $[M, M + \mathrm{d}M]$. We assume that $\phi(M) \sim M^\chi$ with $\chi = -2.35$ as introduced by Salpeter in ref. [100].

JCAP02(2026)069

For the star formation rate history, we take the piecewise broken power-law parametrization by refs. [101, 102]

$$\dot{\rho}_*(z) = \dot{\rho}_0 \left[(1+z)^{\alpha\eta} + \left(\frac{1+z}{B}\right)^{\beta\eta} + \left(\frac{1+z}{C}\right)^{\gamma\eta} \right]^{1/\eta} \tag{6.3}$$

where $\alpha = 3.4$, $\beta = -0.3$, $\gamma = -3.5$ are the logarithmic slopes, $\eta = -10$ is a smoothing parameter and the parameters $B = 5000$ and $C = 9$ define the redshift breaks. The quantity $\dot{\rho}_0$ is the local star formation rate history whose value is adjusted to obtain the desired local core-collapse supernova rate.[10]

One can define the fraction of failed supernovae by

$$f_{\rm BH} = \frac{\int_\Sigma \mathrm{d}M \phi(M)}{\int_{8M_\odot}^{125M_\odot} \mathrm{d}M} \tag{6.4}$$

which was shown to be important in ref. [103] since neutrinos from supernovae leaving a black-hole have higher luminosities and hotter spectra because of the compression of baryonic matter to high densities, thus influencing the tail of the DSNB flux. In our analysis, we considered $f_{\rm BH} = 0.21$ and 0.41 in accordance with the most conservative and optimistic cases found in the extensive detailed supernova simulations of ref. [104]. The current uncertainty on the local core-collapse supernova rate $R_{\rm SN}(0)$ is given by

$$R_{\rm SN}(0) = \int_{8M_\odot}^{125M_\odot} R_{\rm SN}(0, M)\, \mathrm{d}M = (1.25 \pm 0.5) \times 10^{-4}\ \mathrm{y}^{-1}\mathrm{Mpc}^{-3}\,. \tag{6.5}$$

Concerning the cosmological model, we assume the ΛCDM model. For the cosmic time we have

$$\left|\frac{\mathrm{d}t_{\rm c}}{\mathrm{d}z}\right|^{-1} = H_0(1+z)\sqrt{\Omega_\Lambda + (1+z)^3\Omega_m} \tag{6.6}$$

with H_0 the Hubble constant that we take $H_0 = 70$ km s^{-1}Mpc^{-1}, $\Omega_\Lambda = 0.7$ and $\Omega_m = 0.3$ the dark energy and the matter cosmic energy density, respectively.

6.2 The DSNB model

In order to model the contribution from different progenitors M to the DSNB flux, we employed a parametric approach as done in e.g. [26, 27, 105, 106]. More explicitly, we considered supernova templates for different progenitors and equations of state, as in our previous analysis for a future galactic supernova. Note that refs. [102, 107, 108] also employed information from SN1987A to model the DSNB flux, with different approaches and limitations.

Figure 15 presents the progenitor mass intervals and the supernova models used in each of them. For NS-forming collapses, we used models from the Garching group: the 1.36DD2 and 1.44SFHx [46, 47]–with progenitors of $9M_\odot$ and $18.8M_\odot$, respectively–and the s20.0 model with the LS220 equation of state, denoted 20LS220 [46, 55]. Note that for the NS cases, we also considered the 1.62 $M_\odot$, which has an $18.6M_\odot$ progenitor, but the results are insensitive to

[10] See table I in ref. [26] for explicit values.

JCAP02(2026)069

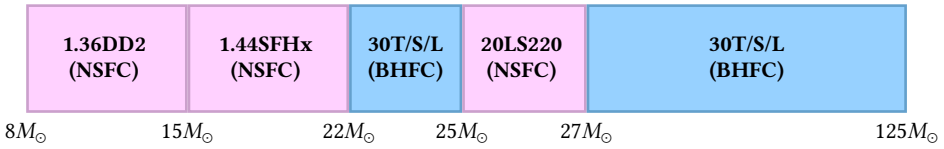

Figure 15. DSNB model: the figure shows the reference models taken in each progenitor mass interval, where the core-collapse supernova leaves either a neutron star or a black hole. For the former, the detailed one-dimensional simulations for SN1987A from the Garching group were used [47] as well as the $20M_\odot$ model from [109]. For the latter, the BH simulation from Nakazato was employed [61]. For the BH cases, the three equations of state were considered, namely the Togashi (T), the Lattimer-Swesty (L), and Shen (S). Note that the same BH template was used for the two mass intervals, i.e., $M \in [22M_\odot, 25M_\odot]$ and $M > 27M_\odot$.

this change. For BH-forming collapses, we used the 30T, 30S, and 30L models from simulations of a $30, M_\odot$ progenitor with different equations of state [48, 49, 61]. We considered three separate scenarios, each using one of these models to represent a BH forming case. The model we adopted corresponds to a fraction of BH $f_{\rm BH} = 0.21$ (as the reference model in our previous work [26]) while we also considered the most optimistic scenario in which $f_{\rm BH} = 0.41$ where we have one NS model with 1.44SFHx for the NS in the range $M \in [8M_\odot, 15M_\odot]$ and one BH model with $30M_\odot$ for the range in $M > 15M_\odot$. We will comment on how our results change when considering the most optimistic scenario for the BH fraction.

To implement the impact of neutrino decay in matter at each individual supernova, we follow the theoretical treatment described in section 2. In particular, we consider that neutrinos start free streaming from the energysphere to the transportspheres in the case of ν_x and $\bar{\nu}_x$ and from the neutrinosphere for $\nu_e, \bar{\nu}_e$ and undergo flux suppression eqs. (2.21)–(2.22) and spectral modification due to decay in these dense stellar regions. Then neutrinos propagate and undergo the MSW effect in the outer stellar layers (2.36)–(2.37). We emphasize that in the inclusion of neutrino decay in matter, we implemented the same time-dependence as in section 2.4. The impact of decay on the neutrino fluxes at individual supernovae is the one described previously, for each neutrino species. From the time-dependent fluxes with and without decay, we build the DSNB fluences.

6.3 Neutrino decay in matter and the DSNB: numerical results

Before giving the DSNB results in the presence of decay, we show the sensitivity of the DSNB fluxes to the BH contribution when the three EOS are considered. This is shown in figure 16 for ν_e, $\bar{\nu}_e$ and the non-electronic neutrino species, for the case of normal ordering. The largest variation reaches up to a factor of a few in the energy range $E_\nu \in [10, 35]$ MeV, from the Lattimer-Swesty EOS and for $\bar{\nu}_e$. It is to be noted, though, that this EOS does not comply with some of the bounds for neutron star matter [110]. Table 7 displays the modifications in the DSNB total number of events, in the different experiments, when varying the EOS. The results are for the two mass orderings and our reference calculations with $f_{\rm BH} = 0.21$. Note that in DARWIN, we find only a couple of DSNB events.

Concerning the impact of decay, figures 17 and 18 show, for normal neutrino mass ordering, the DSNB fluxes for the ν_e and $\bar{\nu}_e$ and the flux ratios of the $\bar{\nu}_e$ and ν_x fluxes with decay over

JCAP02(2026)069

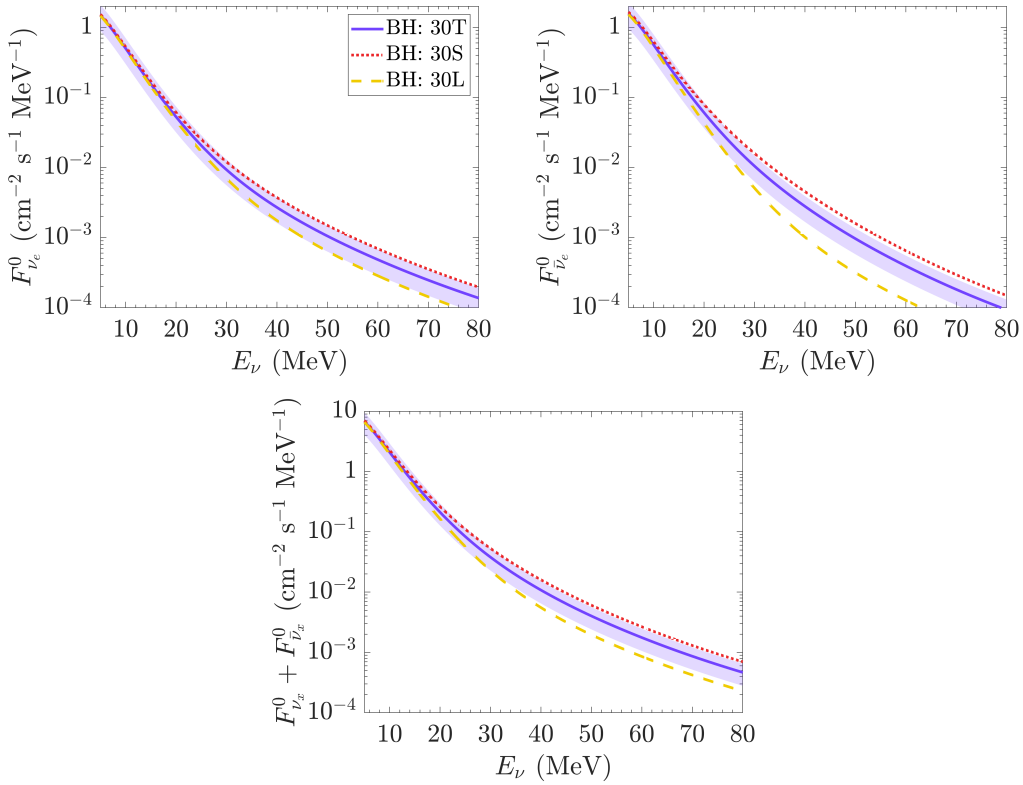

Figure 16. DSNB fluxes in the absence of neutrino decay for the different neutrino species for the case of normal neutrino mass ordering. The different curves show the variations due to changes in the BH template when considering different equations of state, namely the Togashi (T), the Lattimer-Swesty (L), and Shen (S). The bands correspond to the current uncertainty on the evolving core-collapse supernova rate associated with the results of the Shen EOS (see text).

Flux	BH template			Current limits
	30T	30S	30L	
ν_e	0.16 ± 0.07	0.21 ± 0.08	0.13 ± 0.05	19 (SNO)
	(0.16 ± 0.07)	(0.22 ± 0.09)	(0.11 ± 0.04)	
$\bar{\nu}_e$	0.58 ± 0.23	0.80 ± 0.32	0.37 ± 0.15	2.7 (SK)
	(0.52 ± 0.21)	(0.63 ± 0.25)	(0.43 ± 0.17)	
ν_x	1.46 ± 0.58	1.93 ± 0.77	0.99 ± 0.39	$(1.3\text{–}1.8) \times 10^3$
	(1.50 ± 0.60)	(2.03 ± 0.81)	(0.98 ± 0.39)	

Table 6. Integrated DSNB fluxes in normal and inverted ordering (in parentheses), including uncertainties from the core-collapse supernova rate. The flux values (ν/cm^2/s) correspond to the integrated fluxes over the ranges $E_\nu \in [22.9, 36.9]$ MeV for ν_e, $E_\nu > 17.3$ MeV for $\bar{\nu}_e$, and $E_\nu > 19$ MeV for ν_x, and shown for different EOS for the BH model. The last column gives the experimental upper limits on the DSNB fluxes (90% C.L.) from SK [18] and SNO [111]. The loosest bounds on ν_x ($x = \mu, \tau$ flavors) are obtained from [112].

JCAP02(2026)069

	BH template		
	30T	30S	30L
HK-Gd	55 (48)	75 (58)	35 (40)
JUNO	19 (17)	25 (19)	14 (15)
DUNE	9 (9)	10 (11)	7 (6)

Table 7. Expected total number of DSNB events, in the absence of neutrino-Majoron interactions, at several detectors (first column) after 20 years of exposure. The results were obtained using fixed templates for the NS cases and varying the templates for the BH cases between the models 30T (second), 30S (third), and 30L (fourth column). The events are given in normal and inverted ordering (in parentheses). The results for HK-Gd are obtained in the energy window $E_{e^+} \in [16\text{–}30]$ MeV and an efficiency of 0.4. The detection energy window for JUNO is $E_{e^+} \in [11.5\text{–}29.5$ MeV, and we assumed an efficiency of 0.86. For DUNE, we considered $E_\nu \in [19\text{–}31$ MeV and an efficiency of 0.85.

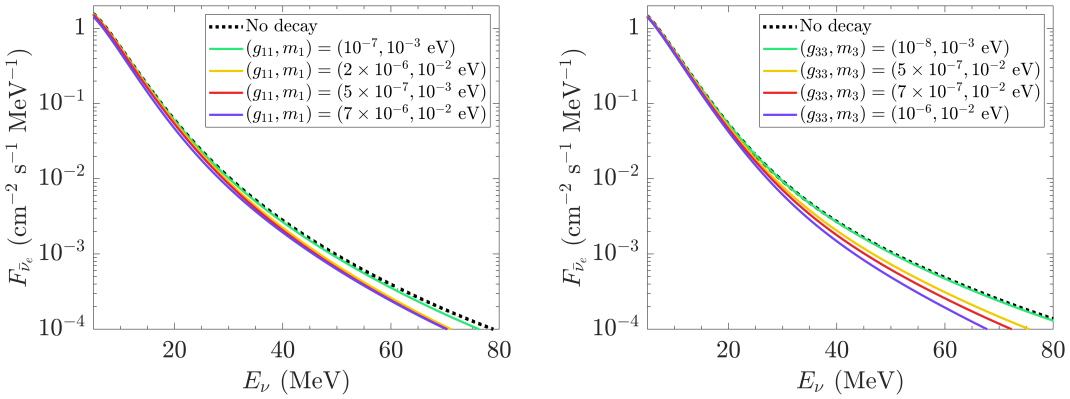

Figure 17. DSNB fluxes for $\bar{\nu}_e$ for normal (left) and inverted (right) mass ordering. The figure compares the fluxes in the absence (dotted) and in the presence (full lines) of decay for different values of neutrino-Majoron coupling g_{11} and lightest neutrino mass m_1 (left) or g_{33} and m_3 (right).

those without decay, respectively. As one can see, neutrino nonradiative decay suppresses the fluxes when the neutrino-Majoron couplings vary from $(g_{11}, m_1) = (10^{-7}, 10^{-3})$ eV to $(7 \times 10^{-6}, 10^{-2})$ eV. This reduction is of less than 10 % for ν_e, of about 30% for ν_x for normal ordering and negligible for the inverted, and between 20–30% for $\bar{\nu}_e$ in the $[10, 30]$ MeV neutrino energy range. Thus one can see that the $\bar{\nu}_e$ and ν_x suppression at high energies found for a single supernova leaving a NS (figure 5) and a BH (figure 6), are reflected in the DSNB predictions, after integrating over redshift and including different progenitors, in our DSNB model. In inverted ordering, the flux suppression in the DSNB region of interest is larger than for normal ordering.

JCAP02(2026)069

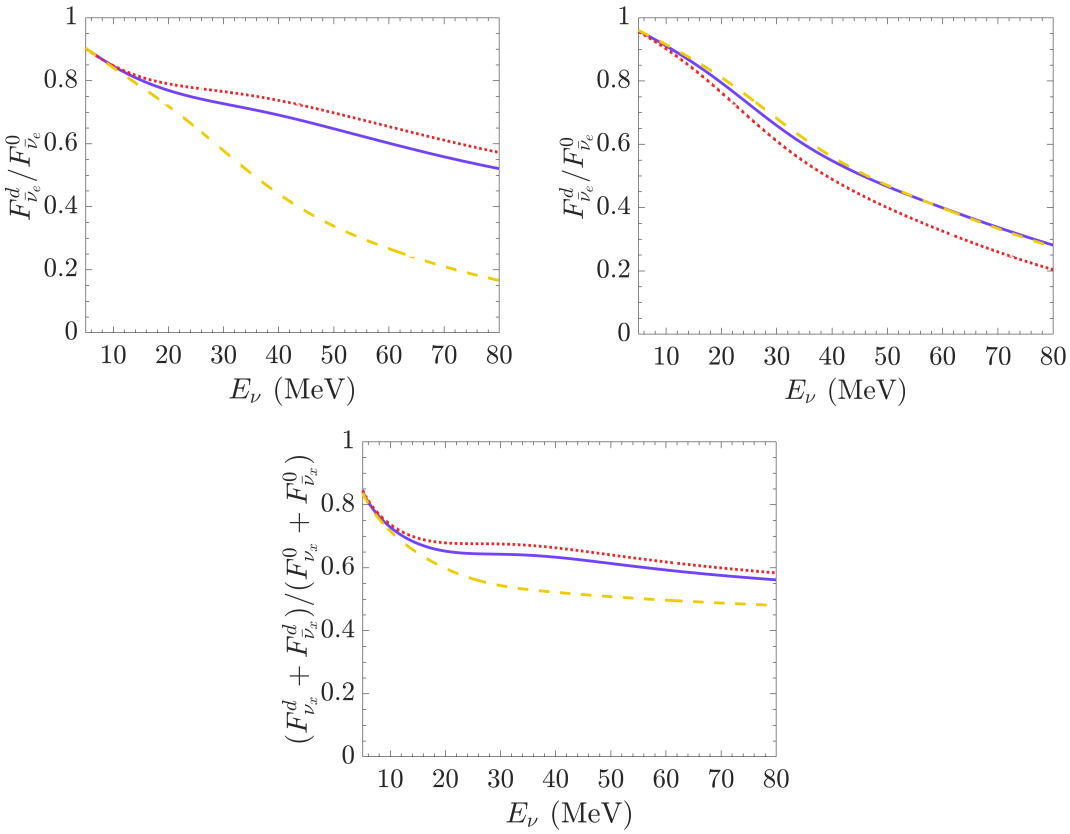

Figure 18. Ratios of the DSNB fluxes with decay over the ones without decay for $\bar{\nu}_e$ for normal (top left) and inverted (top right) mass orderings, as well as for ν_x (bottom figure). The different curves show the variations due to changes in the BH template when considering different equations of state, namely the Togashi (T), the Lattimer-Swesty (L), and Shen (S).

Table 6 presents our integrated DSNB flux predictions, in comparison with the current experimental DSNB bounds on ν_e and $\bar{\nu}_e$ from the SK and SNO experiments. One can see that our results are more than an order of magnitude smaller than the current SK upper limit [18], a factor of more than 20–30 below the ones from SNO and thus are on the conservative side, as the ones in, e.g., refs. [26, 27]. The loosest bounds are those for ν_x.

To predict the number of events in the four experiments, we use the same cross sections for the main detection channels as in section 5.1. The impact of neutrino nonradiative two-body decay in matter on the DSNB number of events is shown in figure 19 for HK with Gadolinium (HK-Gd). Table 7 presents the DSNB expected number of events in HK after 20 years running, for the detection channels. Our results show a decrease in the number of events as a function of positron energy and in the total number of events for HK, while in the other detectors, the DSNB predictions appear to have little sensitivity to this non-standard process. Table 8 shows that the impact of decay on HK-Gd ranges at the level of about 25-30%. While the neutrino decay impact is within the largest uncertainties associated with other factors that determine the DSNB flux, in particular the evolving core-collapse supernova rate, the fluxes at individual supernovae and the fraction of BH (or of binaries, see [104, 113]), its

JCAP02(2026)069

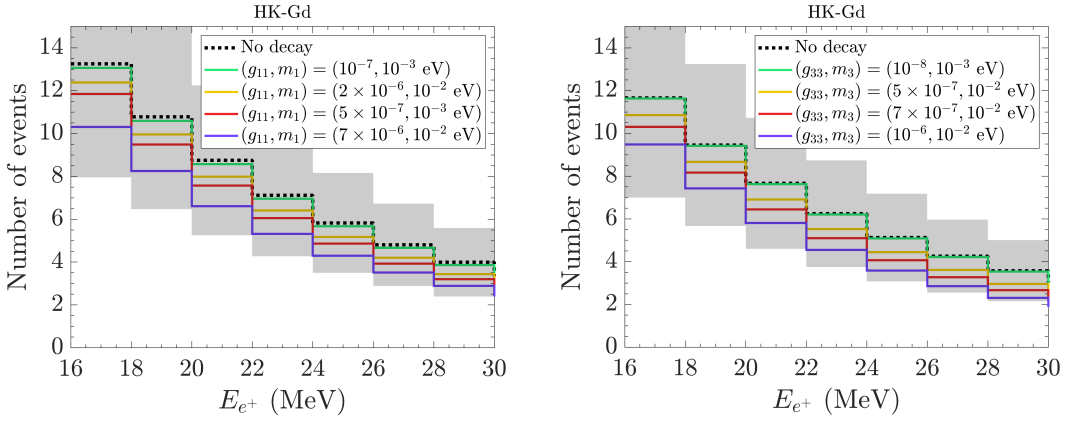

Figure 19. DSNB predictions on the total number of events as a function of positron energy in HK-Gd, after 20 years running. The curves correspond to the case with decay for different values of the neutrino-Majoron couplings g_{11} (g_{33}) as a function of the lightest neutrino mass m_1 (m_3) for normal on the left figure (inverted, right figure) mass ordering. The bands display the uncertainty coming from the evolving core-collapse supernova rate associated with the no decay case (dotted line).

BH template	No decay	Largest effect	Ratio
30T	55	41	0.76
	(48)	(36)	(0.75)
30S	75	59	0.78
	(58)	(41)	(0.71)
30L	35	24	0.68
	(40)	(31)	(0.77)

Table 8. Expected total number of DSNB events at HK-Gd loaded after 20 years of exposure. The results are obtained considering different templates for the BHs. The second column shows the number of events in the absence of decay, while the third and fourth columns correspond to the cases with the largest decay effects and the ratio between the two cases, respectively. Results are given for both normal mass ordering and inverted ordering (in parentheses). The largest decay effects are obtained for $g_{11} = 7 \times 10^{-6}$ and $m_1 = 10^{-2}$ eV for normal ordering and $g_{33} = 10^{-6}$ and $m_3 = 10^{-2}$ eV for inverted ordering. The energy window considered for HK-Gd is $E_{e^+} \in [16, 30]$ MeV and the efficiency is taken as $\eta = 0.4$.

impact is at the same level as aspects pointed out in the literature such as, e.g., shock wave or flavor conversion effects (see [11, 114]).

7 Conclusions

In this work, we have investigated the impact of neutrino non-radiative two-body decay into a massless Majoron, in matter, during a core-collapse supernova explosion, while our results are also of interest for massless or close to massless Majoron-like particles (fuzzy dark matter). The theoretical framework used is the one developed in our previous study ref. [36]. In

JCAP02(2026)069

particular, we consider a full 3ν framework and employ inputs from detailed one-dimensional core-collapse supernova simulations from the Garching group and from Nakazato's simulations. In particular, we have implemented the time-dependence of the neutrino fluxes, the matter densities, and the electron fraction in our microscopic computation of the neutrinospheres, energyspheres, and transportspheres necessary to determine the neutrino flux suppression due to decay.

Based on such a theoretical framework, our investigation has followed three directions. We have first given new limits on neutrino-Majoron couplings using SN1987A observations. Then we have presented our prospects for a future galactic core-collapse supernova obtained from a likelihood analysis exploiting the neutrino spectral distortion due to neutrino nonradiative two-body decay. Besides, we have explored for the first time its impact on the DSNB and shown that it is potentially significant for the HK experiment.

After showing the impact of neutrino decay on the neutrino fluxes, we have first presented new bounds on neutrino-Majoron couplings obtained thanks to a 2-dimensional likelihood analysis of the 24 $\bar{\nu}_e$ events from SN1987A in Kamiokande, IMB, and Baksan. The results shown are both for normal and for inverted neutrino mass ordering. Our bounds vary only slightly when changing model or EOS for the cases considered, and are competitive with the limits from neutrinoless double-beta decay experiments and from the luminosity argument.

Then, we have presented both the total and the expected number of neutrino events as a function of neutrino energy, from a core-collapse supernova in four experiments, namely the JUNO and near future HK experiments, and the more distant future DUNE and DARWIN, showing the impact of neutrino decay for values of the neutrino-Majoron couplings still allowed, also considering our limits from SN1987A. By exploiting the spectral distortions due to neutrino decay in matter, we performed a 2-dimensional likelihood analysis, profiling on the models, to give prospects on the neutrino-Majoron coupling if a core-collapse supernova explodes at different locations in our Milky Way. Such an analysis has shown that a significant improvement on the limits for neutrino-Majoron couplings could be obtained from the next galactic supernova, both if a neutron star or if a black-hole is formed, the latter being the most interesting case.

In our analysis of the impact of neutrino decay in matter on the DSNB, we have employed a DSNB model using the NS and BH detailed simulations used for an individual supernova. Our results show that neutrino decay can suppress the $\bar{\nu}_e$ DSNB flux up to several tens of percent in the energy region of interest and can impact the DSNB number of events in HK-Gd up to 30 % while JUNO, DUNE and DARWIN appear to have negligible sensitivity to this nonstandard process. The effect in HK or HK-Gd does not vary in our case if we increase the BH fraction to the most optimistic value. This is likely due to the limited number of templates included. In our DSNB predictions, the BH contribution is particularly important and dominates the effect from decay. While our findings on the potential sensitivity of HK or HK-Gd to neutrino decay in matter are encouraging, further investigations will be necessary in particular using a more detailed description of the BH contributions and a larger set of EOS when these will become available.

Clearly, several improvements of the presented analysis can be envisaged in the future, e.g., with the implementation of multidimensional supernova simulations, or of a more detailed

JCAP02(2026)069

description, in particular of the BH contribution, for the case of the DSNB. Moreover, a more complete description of neutrino evolution in the presence of Majorons in the supernova core, up to the solution of transport equations, could be envisaged, including neutrino decay in matter. Furthermore, extensions of the presented framework could include more sophisticated flavor conversion effects in the dense regions coming from, e.g., neutrino-neutrino interactions.

While awaiting the next core-collapse supernova in our Galaxy or nearby, the search for the DSNB will continue. The upcoming results from SK, including Gadolinium, and from JUNO, and the start of HK, and DUNE, which have the potential to discover the DSNB, open very exciting times for neutrino astrophysics and the search for new physics. Our investigation unveils new elements of the interesting potential that a future core-collapse supernova and the DSNB have for the process of neutrino nonradiative decay.

Acknowledgments

The authors wish to thank Keníchiro Nakazato for the use of the detailed output from his simulations of the 30 $M_\odot$ supernova leaving a black-hole [48, 49, 61] as well as Thomas Janka, Daniel Kresse, and their collaborators for providing us with information from the one-dimensional simulations for SN1987A ref. [47], giving us access to the Garching archives [46]. The authors acknowledge financial support from the Masterproject NUFRONT of "CNRS Nucléaire et Particules".

A Statistical analysis

In this work, we have considered two types of analysis: the analysis of observed data (SN1987A) and the analysis of future simulated data. For the analysis of SN1987A, we followed closely the procedure described in refs. [21, 71]. Due to the small size of the dataset, we used an unbinned likelihood given by

$$\mathcal{L}(x) = e^{-(S_{\rm tot}(x)+B_{\rm tot})} \times \prod_{i=1}^{N_{\rm obs}} dE \left[\frac{dS}{dE_i}(x) + \frac{dB}{dE_i}\right], \tag{A.1}$$

where x represents the set of parameters describing our model, $S_{\rm tot}$ indicates the expected total number of signal events, and $B_{\rm tot}$ the total background for each detector. The number of observed events, $N_{\rm obs}$, is equal to 11 for Kamiokande-II, 8 for IMB, and 5 for Baksan. The term dS/dE_i represents the expected number of signal events around the observed energies E_i, while the background at those energies is denoted as dB/dE_i. We followed [21] to calculate the expected signal and used the information on the events given there.

In contrast, the next galactic core-collapse supernova is expected to result in a large number of events. Therefore, it is convenient to use a binned Poisson likelihood for the analysis. Dropping the constant terms, the logarithm of the binned likelihood is given by [115]

$$\log \mathcal{L}(x) = -S_{\rm tot}(x) + \sum_{i=1}^{N_{\rm bins}} N_i \log \frac{dS}{dE_i}(x), \tag{A.2}$$

where x denotes the model parameters, $S_{\rm tot}$ the total number of expected events, and $N_{\rm bins}$ is the number of energy bins. The observed number of events in bin i is represented by N_i,

JCAP02(2026)069

while dS/dE_i indicates the expected number of events in that bin. Since we are interested in obtaining prospects for a future supernova detection, we simulate the observed data by computing N_i using a chosen "true" model.

In both of our analyses, for normal ordering, we chose g_{11} and m_1 as the free parameters, while for inverted ordering, we took g_{33} and m_3. The other two couplings were obtained using the relations in eq. (2.2) and eq. (2.3) for normal and inverted ordering, respectively. For the analysis of a future supernova, we additionally considered the core-collapse models as discrete nuisance parameters, and we denote them by $\theta_{\rm SN}$. As a result, the parameters in the analysis of a future supernova are g_{ii}, m_i, and $\theta_{\rm SN}$, with $i = 1$ (3) for normal (inverted) ordering. The profile likelihood is obtained by profiling over the core-collapse models, i.e., searching for the model that maximizes the likelihood for each set of (g_{ii}, m_i):

$$L_p(g_{ii}, m_i) = \max_{\theta_{\rm SN}} \mathcal{L}(g_{ii}, m_i, \theta_{\rm SN}). \tag{A.3}$$

The maximum likelihood, on the other hand, is defined as

$$L_{\rm max} = \mathcal{L}(\hat{g}_{ii}, \hat{m}_i, \hat{\theta}_{\rm SN}) = \max_{g_{ii}, m_i, \theta_{\rm SN}} \mathcal{L}(g_{ii}, m_i, \theta_{\rm SN}), \tag{A.4}$$

where $\hat{g}_{ii}$, $\hat{m}_i$, and $\hat{\theta}_{\rm SN}$ are the maximum likelihood estimators.

B Additional results

This appendix provides additional results for a future supernova. Figure 20 shows the expected number of events in normal ordering for the ES channel at HK and the pES channel at JUNO. For inverted ordering, figure 21 presents the event distributions for the dominant detection channels at HK, JUNO, DUNE, and DARWIN in the BH case. The ES signal at HK and the pES signal at JUNO are omitted in this case, as the impact of neutrino decay on these channels is negligible. Finally, table 9 summarizes the total expected number of events for all experiments and detection channels assuming inverted ordering.

JCAP02(2026)069

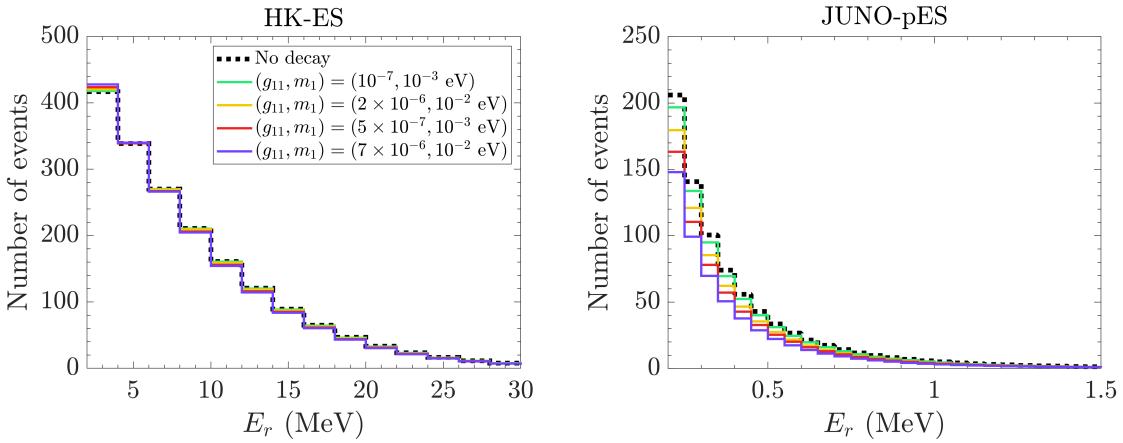

(a) 1.44SFHx (NS).

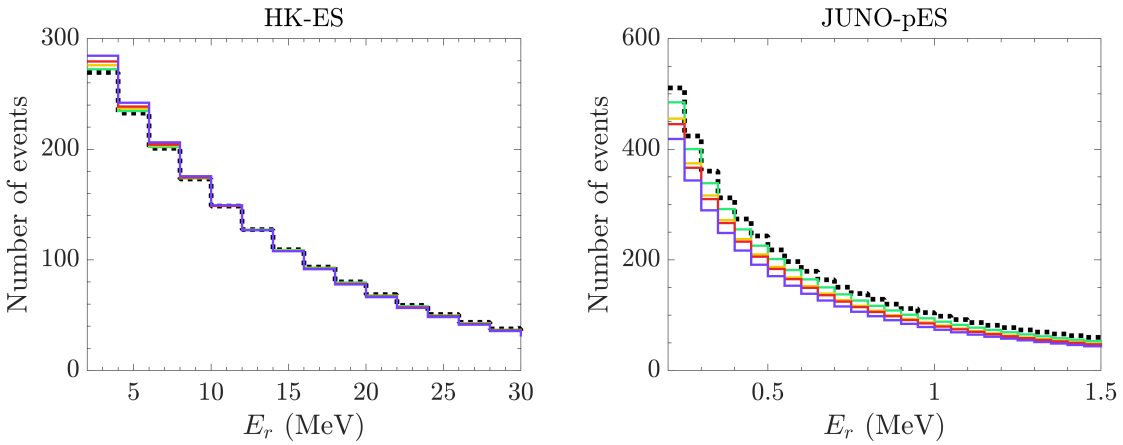

(b) 30T (BH).

Figure 20. Expected events from a future core-collapse supernova located at 10 kpc, assuming normal ordering and including neutrino-Majoron interactions for different values of g_{11} and m_1 compatible with current constraints. Predictions are given for the elastic scattering signal at HK and the proton elastic scattering signal at JUNO for the NS case using the 1.44SFHx model (top panels) and for the BH case using the 30T model (bottom panels). For comparison, the black dotted line shows the prediction in the absence of neutrino-Majoron interactions.

JCAP02(2026)069

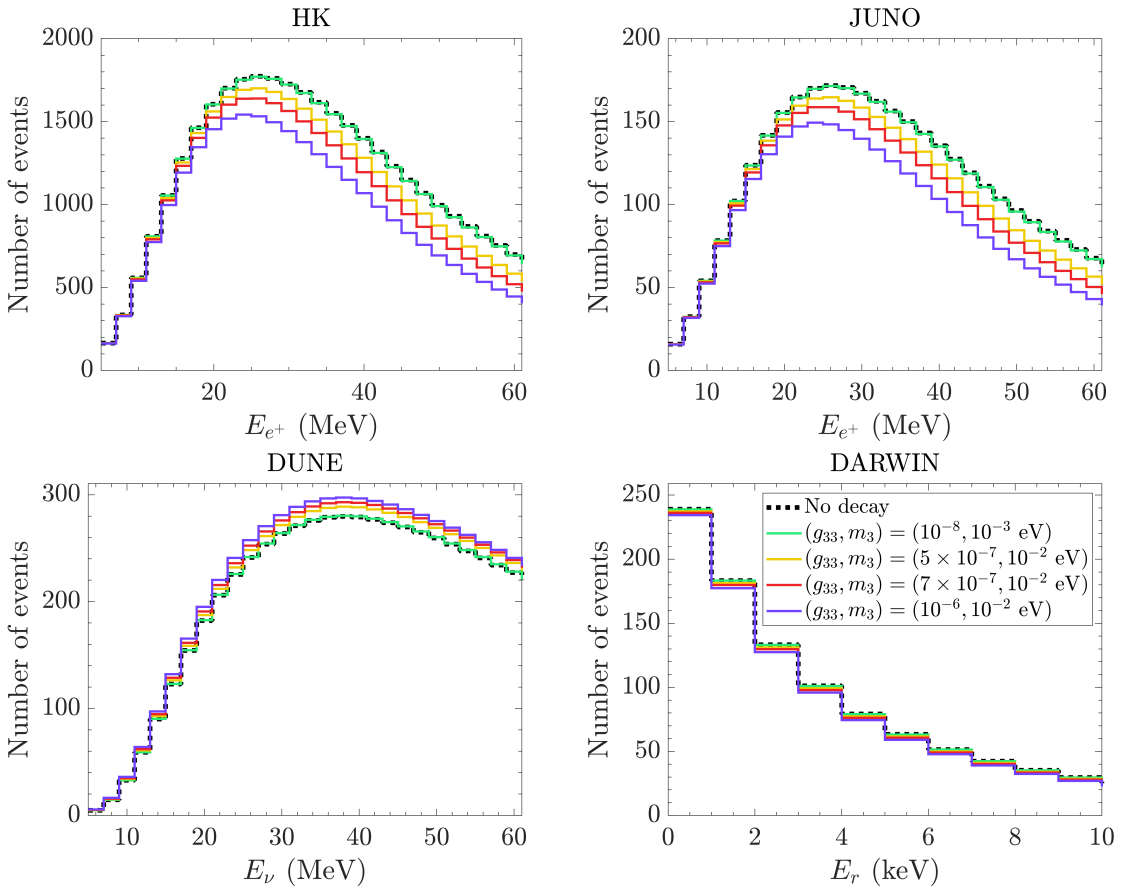

Figure 21. Expected events from a future core-collapse supernova located at 10 kpc, assuming inverted ordering and including neutrino-Majoron interactions for different values of g_{33} and m_3 compatible with current constraints. For comparison, the black dotted line shows the prediction in the absence of neutrino-Majoron interactions. The results were obtained for the BH case using the 30T model. The predictions correspond to the following cases. Upper figures: inverse beta decay events in HK (left) and JUNO (right). Bottom figures: ν-Ar scattering in DUNE (left), coherent neutrino-nucleus scattering in DARWIN (right).

JCAP02(2026)069

	No decay	$g_{33} = 10^{-8}$ $m_3 = 10^{-3}$ eV	$g_{33} = 5 \times 10^{-7}$ $m_3 = 10^{-2}$ eV	$g_{33} = 7 \times 10^{-7}$ $m_3 = 10^{-2}$ eV	$g_{33} = 10^{-6}$ $m_3 = 10^{-2}$ eV
HK-IBD	27884	27868	27438	27046	26304
	(42560)	(42291)	(37850)	(35339)	(31888)
HK-ES	1169	1169	1168	1167	1164
	(1631)	(1631)	(1628)	(1624)	(1617)
JUNO-IBD	2700	2698	2656	2618	2547
	(4120)	(4094)	(3664)	(3421)	(3087)
JUNO-pES	459	459	448	439	423
	(3997)	(3989)	(3829)	(3728)	(3597)
DUNE	2136	2137	2146	2155	2170
	(10982)	(11018)	(11392)	(11514)	(11631)
DARWIN	406	406	402	399	393
	(870)	(869)	(845)	(830)	(810)

Table 9. Expected total number of events from a future supernova located at 10 kpc including neutrino-Majoron interactions producing neutrino nonradiative two-body decay in matter. The results are for the case of inverted mass ordering. The first column shows the detection channels of the four experiments considered. The second column the results in absence of decay, while the other columns give the expected values for different values of the neutrino-Majoron couplings g_{33} and the lightest neutrino mass m_3. The values correspond to the NS case with the 1.44SFHx model and to the BH case with the 30T model (in parenthesis).

References

[1] R. Davis Jr., D.S. Harmer and K.C. Hoffman, *Search for neutrinos from the sun*, *Phys. Rev. Lett.* **20** (1968) 1205 [INSPIRE].

[2] KAMIOKANDE-II collaboration, *Observation of a neutrino burst from the supernova SN 1987a*, *Phys. Rev. Lett.* **58** (1987) 1490 [INSPIRE].

[3] R.M. Bionta et al., *Observation of a neutrino burst in coincidence with supernova SN 1987a in the Large Magellanic Cloud*, *Phys. Rev. Lett.* **58** (1987) 1494 [INSPIRE].

[4] E.N. Alekseev, L.N. Alekseeva, I.V. Krivosheina and V.I. Volchenko, *Detection of the neutrino signal from SN1987A in the LMC using the Inr Baksan underground scintillation telescope*, *Phys. Lett. B* **205** (1988) 209 [INSPIRE].

[5] LIGO SCIENTIFIC et al. collaborations, *Multi-messenger observations of a binary neutron star merger*, *Astrophys. J. Lett.* **848** (2017) L12 [arXiv:1710.05833] [INSPIRE].

[6] ICECUBE collaboration, *Observation of high-energy astrophysical neutrinos in three years of IceCube data*, *Phys. Rev. Lett.* **113** (2014) 101101 [arXiv:1405.5303] [INSPIRE].

[7] KM3NET collaboration, *Observation of an ultra-high-energy cosmic neutrino with KM3NeT*, *Nature* **638** (2025) 376 [*Erratum ibid.* **640** (2025) E3] [INSPIRE].

[8] SUPER-KAMIOKANDE collaboration, *Evidence for oscillation of atmospheric neutrinos*, *Phys. Rev. Lett.* **81** (1998) 1562 [hep-ex/9807003] [INSPIRE].

JCAP02(2026)069

[9] Particle Data Group collaboration, *Review of particle physics*, *Phys. Rev. D* **110** (2024) 030001 [INSPIRE].

[10] J.T. Pantaleone, *Neutrino oscillations at high densities*, *Phys. Lett. B* **287** (1992) 128 [INSPIRE].

[11] M.C. Volpe, *Neutrinos from dense environments: flavor mechanisms, theoretical approaches, observations, and new directions*, *Rev. Mod. Phys.* **96** (2024) 025004 [arXiv:2301.11814] [INSPIRE].

[12] C. Volpe, *Neutrino quantum kinetic equations*, *Int. J. Mod. Phys. E* **24** (2015) 1541009 [arXiv:1506.06222] [INSPIRE].

[13] I. Tamborra and S. Shalgar, *New developments in flavor evolution of a dense neutrino gas*, *Ann. Rev. Nucl. Part. Sci.* **71** (2021) 165 [arXiv:2011.01948] [INSPIRE].

[14] H. Duan, G.M. Fuller and Y.-Z. Qian, *Collective neutrino oscillations*, *Ann. Rev. Nucl. Part. Sci.* **60** (2010) 569 [arXiv:1001.2799] [INSPIRE].

[15] PandaX collaboration, *First indication of solar B^8 neutrinos through coherent elastic neutrino-nucleus scattering in PandaX-4T*, *Phys. Rev. Lett.* **133** (2024) 191001 [arXiv:2407.10892] [INSPIRE].

[16] XENON collaboration, *First indication of solar B^8 neutrinos via coherent elastic neutrino-nucleus scattering with XENONnT*, *Phys. Rev. Lett.* **133** (2024) 191002 [arXiv:2408.02877] [INSPIRE].

[17] K. Rozwadowska, F. Vissani and E. Cappellaro, *On the rate of core collapse supernovae in the Milky Way*, *New Astron.* **83** (2021) 101498 [arXiv:2009.03438] [INSPIRE].

[18] Super-Kamiokande collaboration, *Diffuse supernova neutrino background search at Super-Kamiokande*, *Phys. Rev. D* **104** (2021) 122002 [arXiv:2109.11174] [INSPIRE].

[19] A. Beauchene, private communication.

[20] J.F. Beacom and M.R. Vagins, *GADZOOKS! Antineutrino spectroscopy with large water Cherenkov detectors*, *Phys. Rev. Lett.* **93** (2004) 171101 [hep-ph/0309300] [INSPIRE].

[21] P. Iváñez-Ballesteros and M.C. Volpe, *SN1987A and neutrino non-radiative decay*, *Phys. Lett. B* **847** (2023) 138252 [arXiv:2307.03549] [INSPIRE].

[22] M. Escudero and S.J. Witte, *A CMB search for the neutrino mass mechanism and its relation to the Hubble tension*, *Eur. Phys. J. C* **80** (2020) 294 [arXiv:1909.04044] [INSPIRE].

[23] T. Brune and H. Päs, *Massive Majorons and constraints on the Majoron-neutrino coupling*, *Phys. Rev. D* **99** (2019) 096005 [arXiv:1808.08158] [INSPIRE].

[24] G.L. Fogli, E. Lisi, A. Mirizzi and D. Montanino, *Three generation flavor transitions and decays of supernova relic neutrinos*, *Phys. Rev. D* **70** (2004) 013001 [hep-ph/0401227] [INSPIRE].

[25] A. De Gouvêa, I. Martinez-Soler, Y.F. Perez-Gonzalez and M. Sen, *Fundamental physics with the diffuse supernova background neutrinos*, *Phys. Rev. D* **102** (2020) 123012 [arXiv:2007.13748] [INSPIRE].

[26] P. Iváñez-Ballesteros and M.C. Volpe, *Neutrino nonradiative decay and the diffuse supernova neutrino background*, *Phys. Rev. D* **107** (2023) 023017 [arXiv:2209.12465] [INSPIRE].

[27] N. Roux and M.C. Volpe, *Diffuse supernova neutrino background and neutrino non-radiative decay: a Bayesian perspective*, *JCAP* **04** (2025) 021 [arXiv:2412.14681] [INSPIRE].

[28] E.W. Kolb and M.S. Turner, *Supernova 1987A and the secret interactions of neutrinos*, *Phys. Rev. D* **36** (1987) 2895 [INSPIRE].

JCAP02(2026)069

[29] P. Martínez-Miravé, I. Tamborra and M. Tórtola, *The Sun and core-collapse supernovae are leading probes of the neutrino lifetime*, *JCAP* **05** (2024) 002 [arXiv:2402.00116] [INSPIRE].

[30] K. Akita, S.H. Im and M. Masud, *Probing non-standard neutrino interactions with a light boson from next galactic and diffuse supernova neutrinos*, *JHEP* **12** (2022) 050 [arXiv:2206.06852] [INSPIRE].

[31] D.F.G. Fiorillo, G.G. Raffelt and E. Vitagliano, *Strong supernova 1987A constraints on bosons decaying to neutrinos*, *Phys. Rev. Lett.* **131** (2023) 021001 [arXiv:2209.11773] [INSPIRE].

[32] B. Telalovic et al., *The next galactic supernova can uncover mass and couplings of particles decaying to neutrinos*, *JCAP* **11** (2024) 011 [arXiv:2406.15506] [INSPIRE].

[33] M. Kachelriess, R. Tomàs and J.W.F. Valle, *Supernova bounds on Majoron emitting decays of light neutrinos*, *Phys. Rev. D* **62** (2000) 023004 [hep-ph/0001039] [INSPIRE].

[34] R. Tomàs, H. Päs and J.W.F. Valle, *Generalized bounds on Majoron-neutrino couplings*, *Phys. Rev. D* **64** (2001) 095005 [hep-ph/0103017] [INSPIRE].

[35] Y. Farzan, *Bounds on the coupling of the Majoron to light neutrinos from supernova cooling*, *Phys. Rev. D* **67** (2003) 073015 [hep-ph/0211375] [INSPIRE].

[36] P. Iváñez-Ballesteros and M.C. Volpe, *Constraints on neutrino-Majoron coupling using SN1987A data*, *Phys. Rev. D* **112** (2025) L101301 [arXiv:2410.11517] [INSPIRE].

[37] M. Aglietta et al., *On the event observed in the Mont Blanc Underground Neutrino observatory during the occurrence of supernova 1987a*, *EPL* **3** (1987) 1315 [INSPIRE].

[38] J.Z. Chen, I.M. Oldengott, G. Pierobon and Y.Y.Y. Wong, *Weaker yet again: mass spectrum-consistent cosmological constraints on the neutrino lifetime*, *Eur. Phys. J. C* **82** (2022) 640 [arXiv:2203.09075] [INSPIRE].

[39] G.M. Fuller, R. Mayle and J.R. Wilson, *The Majoron model and stellar collapse*, *Astrophys. J.* **332** (1988) 826 [INSPIRE].

[40] A.M. Suliga et al., *Nonconservation of lepton numbers in the neutrino sector could change the prospects for core collapse supernova explosions*, *Phys. Rev. Lett.* **134** (2025) 241002 [arXiv:2410.01080] [INSPIRE].

[41] Y. Chikashige, R.N. Mohapatra and R.D. Peccei, *Spontaneously broken lepton number and cosmological constraints on the neutrino mass spectrum*, *Phys. Rev. Lett.* **45** (1980) 1926 [INSPIRE].

[42] G.B. Gelmini and M. Roncadelli, *Left-handed neutrino mass scale and spontaneously broken lepton number*, *Phys. Lett. B* **99** (1981) 411 [INSPIRE].

[43] E. Baron et al., *Type II supernovae from prompt explosions*, *Phys. Rev. Lett.* **59** (1987) 736 [INSPIRE].

[44] C. Giunti, C.W. Kim, U.W. Lee and W.P. Lam, *Majoron decay of neutrinos in matter*, *Phys. Rev. D* **45** (1992) 1557 [INSPIRE].

[45] G.-Y. Huang, T. Ohlsson and S. Zhou, *Observational constraints on secret neutrino interactions from Big Bang nucleosynthesis*, *Phys. Rev. D* **97** (2018) 075009 [arXiv:1712.04792] [INSPIRE].

[46] M. Harada, *The Garching core-collapse supernova archive*, https://wwwmpa.mpa-garching.mpg.de/ccsnarchive/.

[47] D.F.G. Fiorillo et al., *Supernova simulations confront SN 1987A neutrinos*, *Phys. Rev. D* **108** (2023) 083040 [arXiv:2308.01403] [INSPIRE].

JCAP02(2026)069

[48] K. Nakazato et al., *Supernova neutrino light curves and spectra for various progenitor stars: from core collapse to proto-neutron star cooling*, *Astrophys. J. Suppl.* **205** (2013) 2 [arXiv:1210.6841] [INSPIRE].

[49] K. Nakazato, K. Sumiyoshi and H. Togashi, *Numerical study of stellar core collapse and neutrino emission using the nuclear equation of state obtained by the variational method*, *Publ. Astron. Soc. Jap.* **73** (2021) 639 [arXiv:2103.14386] [INSPIRE].

[50] *Supernova Neutrino Database webpage*, http://asphwww.ph.noda.tus.ac.jp/snn/.

[51] J. Schechter and J.W.F. Valle, *Neutrino decay and spontaneous violation of lepton number*, *Phys. Rev. D* **25** (1982) 774 [INSPIRE].

[52] Z.G. Berezhiani and M.I. Vysotsky, *Neutrino decay in matter*, *Phys. Lett. B* **199** (1987) 281 [INSPIRE].

[53] L. Wolfenstein, *Neutrino oscillations in matter*, *Phys. Rev. D* **17** (1978) 2369 [INSPIRE].

[54] S.P. Mikheev and A.Y. Smirnov, *Resonant amplification of neutrino oscillations in matter and solar neutrino spectroscopy*, *Nuovo Cim. C* **9** (1986) 17 [INSPIRE].

[55] R. Bollig et al., *Muon creation in supernova matter facilitates neutrino-driven explosions*, *Phys. Rev. Lett.* **119** (2017) 242702 [arXiv:1706.04630] [INSPIRE].

[56] Z.G. Berezhiani and A.Y. Smirnov, *Matter induced neutrino decay and supernova SN1987A*, *Phys. Lett. B* **220** (1989) 279 [INSPIRE].

[57] H. Nunokawa, J.T. Peltoniemi, A. Rossi and J.W.F. Valle, *Supernova bounds on resonant active sterile neutrino conversions*, *Phys. Rev. D* **56** (1997) 1704 [hep-ph/9702372] [INSPIRE].

[58] G.G. Raffelt, *Muon-neutrino and tau-neutrino spectra formation in supernovae*, *Astrophys. J.* **561** (2001) 890 [astro-ph/0105250] [INSPIRE].

[59] S.L. Shapiro and S.A. Teukolsky, *Black holes, white dwarfs, and neutron stars: the physics of compact objects*, Wiley (1983) [DOI:10.1002/9783527617661] [INSPIRE].

[60] M.T. Keil, G.G. Raffelt and H.-T. Janka, *Monte Carlo study of supernova neutrino spectra formation*, *Astrophys. J.* **590** (2003) 971 [astro-ph/0208035] [INSPIRE].

[61] K. Nakazato, private communication.

[62] M. Cornelius, S. Shalgar and I. Tamborra, *Perturbing fast neutrino flavor conversion*, *JCAP* **02** (2024) 038 [arXiv:2312.03839] [INSPIRE].

[63] D.F.G. Fiorillo, H.-T. Janka and G.G. Raffelt, *Neutrino-mass-driven instabilities as the earliest flavor conversion in supernovae*, *Phys. Rev. Lett.* **135** (2025) 231003 [arXiv:2507.22985] [INSPIRE].

[64] D.F.G. Fiorillo and G.G. Raffelt, *Collective flavor conversions are interactions of neutrinos with quantized flavor waves*, *Phys. Rev. Lett.* **134** (2025) 211003 [arXiv:2502.06935] [INSPIRE].

[65] H.A. Bethe and J.R. Wilson, *Revival of a stalled supernova shock by neutrino heating*, *Astrophys. J.* **295** (1985) 14 [INSPIRE].

[66] C. Kato, K. Ishidoshiro and T. Yoshida, *Theoretical prediction of presupernova neutrinos and their detection*, *Ann. Rev. Nucl. Part. Sci.* **70** (2020) 121 [arXiv:2006.02519] [INSPIRE].

[67] S.W. Li, J.F. Beacom, L.F. Roberts and F. Capozzi, *Old data, new forensics: the first second of SN 1987A neutrino emission*, *Phys. Rev. D* **109** (2024) 083025 [arXiv:2306.08024] [INSPIRE].

[68] A.W. Steiner, M. Hempel and T. Fischer, *Core-collapse supernova equations of state based on neutron star observations*, *Astrophys. J.* **774** (2013) 17 [arXiv:1207.2184] [INSPIRE].

JCAP02(2026)069

[69] M. Hempel and J. Schaffner-Bielich, *Statistical model for a complete supernova equation of state*, *Nucl. Phys. A* **837** (2010) 210 [arXiv:0911.4073] [INSPIRE].

[70] A. Gallo Rosso, F. Vissani and M.C. Volpe, *What can we learn on supernova neutrino spectra with water Cherenkov detectors?*, *JCAP* **04** (2018) 040 [arXiv:1712.05584] [INSPIRE].

[71] F. Vissani, *Comparative analysis of SN1987A antineutrino fluence*, *J. Phys. G* **42** (2015) 013001 [arXiv:1409.4710] [INSPIRE].

[72] S.A. Kharusi et al., *Search for Majoron-emitting modes of ^{136}Xe double beta decay with the complete EXO-200 dataset*, *Phys. Rev. D* **104** (2021) 112002 [arXiv:2109.01327] [INSPIRE].

[73] KATRIN collaboration, *Direct neutrino-mass measurement based on 259 days of KATRIN data*, *Science* **388** (2025) adq9592 [arXiv:2406.13516] [INSPIRE].

[74] KamLAND-Zen collaboration, *Limits on Majoron-emitting double-beta decays of ^{136}Xe in the KamLAND-Zen experiment*, *Phys. Rev. C* **86** (2012) 021601 [arXiv:1205.6372] [INSPIRE].

[75] NEMO-3 collaboration, *Results of the search for neutrinoless double-β decay in ^{100}Mo with the NEMO-3 experiment*, *Phys. Rev. D* **92** (2015) 072011 [arXiv:1506.05825] [INSPIRE].

[76] CUPID-0 collaboration, *Search for Majoron-like particles with CUPID-0*, *Phys. Rev. D* **107** (2023) 032006 [arXiv:2209.09490] [INSPIRE].

[77] GERDA collaboration, *Search for exotic physics in double-β decays with GERDA phase II*, *JCAP* **12** (2022) 012 [arXiv:2209.01671] [INSPIRE].

[78] CUPID collaboration, *Searching for beyond the Standard Model physics using the improved description of ^{100}Mo $2\nu\beta\beta$ decay spectral shape with CUPID-Mo*, *Eur. Phys. J. C* **84** (2024) 925 [arXiv:2405.10766] [INSPIRE].

[79] PIENU collaboration, *Search for three body pion decays $\pi^+ \to l^+ \nu X$*, *Phys. Rev. D* **103** (2021) 052006 [arXiv:2101.07381] [INSPIRE].

[80] A.P. Lessa and O.L.G. Peres, *Revising limits on neutrino-Majoron couplings*, *Phys. Rev. D* **75** (2007) 094001 [hep-ph/0701068] [INSPIRE].

[81] R.F. Lang et al., *Supernova neutrino physics with xenon dark matter detectors: a timely perspective*, *Phys. Rev. D* **94** (2016) 103009 [arXiv:1606.09243] [INSPIRE].

[82] H.-K. Proto-Collaboration et al., *Hyper-Kamiokande design report*, arXiv:1805.04163.

[83] JUNO collaboration, *Neutrino physics with JUNO*, *J. Phys. G* **43** (2016) 030401 [arXiv:1507.05613] [INSPIRE].

[84] DUNE collaboration, *Deep Underground Neutrino Experiment (DUNE), far detector technical design report. Volume I. Introduction to DUNE*, 2020 *JINST* **15** T08008 [arXiv:2002.02967] [INSPIRE].

[85] DARWIN collaboration, *DARWIN: towards the ultimate dark matter detector*, *JCAP* **11** (2016) 017 [arXiv:1606.07001] [INSPIRE].

[86] A. Strumia and F. Vissani, *Precise quasielastic neutrino/nucleon cross-section*, *Phys. Lett. B* **564** (2003) 42 [astro-ph/0302055] [INSPIRE].

[87] G. Ricciardi, N. Vignaroli and F. Vissani, *An accurate evaluation of electron (anti-)neutrino scattering on nucleons*, *JHEP* **08** (2022) 212 [arXiv:2206.05567] [INSPIRE].

[88] A. de Gouvea, P.A.N. Machado, Y.F. Perez-Gonzalez and Z. Tabrizi, *Measuring the weak mixing angle in the DUNE near detector complex*, *Phys. Rev. Lett.* **125** (2020) 051803 [arXiv:1912.06658] [INSPIRE].

JCAP02(2026)069

[89] J.F. Beacom, W.M. Farr and P. Vogel, *Detection of supernova neutrinos by neutrino proton elastic scattering*, *Phys. Rev. D* **66** (2002) 033001 [hep-ph/0205220] [INSPIRE].

[90] *SNOwGLoBES: SuperNova Observatories with GLoBES*, https://github.com/SNOwGLoBES/snowglobes/tree/master/xscns.

[91] SUPER-KAMIOKANDE collaboration, *Solar neutrino results in Super-Kamiokande-III*, *Phys. Rev. D* **83** (2011) 052010 [arXiv:1010.0118] [INSPIRE].

[92] HYPER-KAMIOKANDE collaboration, *Supernova model discrimination with Hyper-Kamiokande*, *Astrophys. J.* **916** (2021) 15 [arXiv:2101.05269] [INSPIRE].

[93] B. Dasgupta and J.F. Beacom, *Reconstruction of supernova ν_μ, ν_τ, anti-ν_μ, and anti-ν_τ neutrino spectra at scintillator detectors*, *Phys. Rev. D* **83** (2011) 113006 [arXiv:1103.2768] [INSPIRE].

[94] B. von Krosigk et al., *Measurement of the proton light response of various LAB based scintillators and its implication for supernova neutrino detection via neutrino-proton scattering*, *Eur. Phys. J. C* **73** (2013) 2390 [arXiv:1301.6403] [INSPIRE].

[95] DUNE collaboration, *Supernova neutrino burst detection with the Deep Underground Neutrino Experiment*, *Eur. Phys. J. C* **81** (2021) 423 [arXiv:2008.06647] [INSPIRE].

[96] COHERENT collaboration, *Observation of coherent elastic neutrino-nucleus scattering*, *Science* **357** (2017) 1123 [arXiv:1708.01294] [INSPIRE].

[97] D.Z. Freedman, *Coherent neutrino nucleus scattering as a probe of the weak neutral current*, *Phys. Rev. D* **9** (1974) 1389 [INSPIRE].

[98] M. Schumann et al., *Dark matter sensitivity of multi-ton liquid xenon detectors*, *JCAP* **10** (2015) 016 [arXiv:1506.08309] [INSPIRE].

[99] C. Lunardini et al., *The diffuse supernova neutrino background: an update with modern population synthesis and core-collapse simulations*, *Phys. Rev. D* (2026) accepted [arXiv:2506.22699] [INSPIRE].

[100] E.E. Salpeter, *The luminosity function and stellar evolution*, *Astrophys. J.* **121** (1955) 161 [INSPIRE].

[101] H. Yuksel, M.D. Kistler, J.F. Beacom and A.M. Hopkins, *Revealing the high-redshift star formation rate with gamma-ray bursts*, *Astrophys. J. Lett.* **683** (2008) L5 [arXiv:0804.4008] [INSPIRE].

[102] S. Horiuchi, J.F. Beacom and E. Dwek, *The diffuse supernova neutrino background is detectable in Super-Kamiokande*, *Phys. Rev. D* **79** (2009) 083013 [arXiv:0812.3157] [INSPIRE].

[103] C. Lunardini, *Diffuse neutrino flux from failed supernovae*, *Phys. Rev. Lett.* **102** (2009) 231101 [arXiv:0901.0568] [INSPIRE].

[104] D. Kresse, T. Ertl and H.-T. Janka, *Stellar collapse diversity and the diffuse supernova neutrino background*, *Astrophys. J.* **909** (2021) 169 [arXiv:2010.04728] [INSPIRE].

[105] A. Priya and C. Lunardini, *Diffuse neutrinos from luminous and dark supernovae: prospects for upcoming detectors at the $O(10)$ kt scale*, *JCAP* **11** (2017) 031 [arXiv:1705.02122] [INSPIRE].

[106] K. Møller, A.M. Suliga, I. Tamborra and P.B. Denton, *Measuring the supernova unknowns at the next-generation neutrino telescopes through the diffuse neutrino background*, *JCAP* **05** (2018) 066 [arXiv:1804.03157] [INSPIRE].

[107] C. Lunardini, *The diffuse supernova neutrino flux, supernova rate and SN1987A*, *Astropart. Phys.* **26** (2006) 190 [astro-ph/0509233] [INSPIRE].

JCAP02(2026)069

[108] F. Vissani and G. Pagliaroli, *The diffuse supernova neutrino background: expectations and uncertainties derived from SN1987A*, *Astron. Astrophys.* **528** (2011) L1 [arXiv:1102.0447] [INSPIRE].

[109] L. Hudepohl, *Neutrinos from the formation, cooling and black hole collapse of neutron stars*, Ph.D. thesis, Munich Tech. U., Munich, Germany (2013) [INSPIRE].

[110] I. Tews, J.M. Lattimer, A. Ohnishi and E.E. Kolomeitsev, *Symmetry parameter constraints from a lower bound on neutron-matter energy*, *Astrophys. J.* **848** (2017) 105 [arXiv:1611.07133] [INSPIRE].

[111] SNO collaboration, *A search for neutrinos from the solar HEP reaction and the diffuse supernova neutrino background with the Sudbury Neutrino Observatory*, *Astrophys. J.* **653** (2006) 1545 [hep-ex/0607010] [INSPIRE].

[112] C. Lunardini and O.L.G. Peres, *Upper limits on the diffuse supernova neutrino flux from the SuperKamiokande data*, *JCAP* **08** (2008) 033 [arXiv:0805.4225] [INSPIRE].

[113] S. Horiuchi et al., *Impact of binary interactions on the diffuse supernova neutrino background*, *Phys. Rev. D* **103** (2021) 043003 [arXiv:2012.08524] [INSPIRE].

[114] G.J. Mathews, L. Boccioli, J. Hidaka and T. Kajino, *Review of uncertainties in the cosmic supernova relic neutrino background*, *Mod. Phys. Lett. A* **35** (2020) 2030011 [arXiv:1907.10088] [INSPIRE].

[115] G. Cowan, *Statistical data analysis*, (1998).

JCAP02(2026)069